1

The march of the human footprint

Eric W. Sanderson*, Kim Fisher, Nathaniel Robinson, Dustin Sampson, Adam Duncan, and

Lucinda Royte

*corresponding author

Author Affiliations

Eric W. Sanderson, Kim Fisher, Adam Duncan, and Lucinda Royte

Wildlife Conservation Society, Bronx, New York, USA

Email: esanderson@wcs.org, kfisher@wcs.org, aduncan@wcs.org, lroyte@wcs.org

Nathaniel Robinson

Panthera, New York, New York, USA

Present address: The Nature Conservancy, Arlington, Virginia, USA

Email: n.robinson@tnc.org

Dustin Sampson

Sparkgeo Consulting Inc., Prince George, British Columbia, Canada

Email: dustin@sparkgeo.com

23 **The march of the human footprint**

24 **Abstract**

25 Human influence is driving planetary change, often in undesirable and unsustainable ways.

26 Recent advances enabled us to measure changes in humanity's footprint on Earth annually from

27 2000 – 2019 with a nine-fold improvement in spatial resolution over previous efforts. We found

28 that earlier studies seriously under-estimated the magnitude, extent, and rate of change in the

29 human footprint. Inclusion of newly available data sources suggest that human influence on the

30 land surface grew faster in the five years prior to the COVID-19 pandemic than at any other time

31 in the last 12,000 years. The global extent of uninfluenced areas declined by 23% over the last

32 two decades, an area equivalent to one-third the land mass of the United States. By providing a

33 mechanism to regularly update maps going forward, this work provides a foundation for more

34 accurate, detailed and timely approaches to sustainability.

35 **Main**

36 As a species, human beings are agents of change[1]. Whereas most species must adapt to the

37 environment in which they find themselves, people adapt the environment to our liking, working

38 in voluble and fluid social groups to advance our aims. We erect structures to facilitate our

39 endeavors and avoid the weather; transform ecosystems to produce foods and materials; extend

40 roads, railways and ports to acquire natural resources and move people and goods; and deploy

41 power to light our nights, heat and cool our buildings, cook our food, and animate our electronic

42 and mechanical helpers.

43 Unfortunately, the combined effect of these structures and activities has had profound

44 consequences for the planet on which we all depend[2-6]. To model these effects scientists have

2

45   discovered that a surprisingly simple index, the human footprint[7,8], has remarkable value[9]. The

46   human footprint is simply the weighted sum of where people live (population density), where we

47   build our infrastructure (roads, railways, and other built infrastructure), where we can reach

48   (accessibility), and where we deploy energy, as measured by the night-time lights data visible

49   from satellites, a proxy for access to industrial energy sources (see Methods). Relative weights

50   transform these disparate, spatial data into a common, synthetic index. Since first described in

51   2002[7], a vast literature has grown up around the human footprint, demonstrating its utility in

52   understanding the distribution and abundance of species,[10,11] measuring the invasibility of

53   landscapes[12,13], loss and fragmentation of natural ecosystems[14,15], changes in the climate through

54   land use change[16] and greenhouse gas emissions[17], and as a general marker of human impacts on

55   the planet[9,18]. Analogous research has shown that relatively uninfluenced areas, conversely, act

56   as carbon sinks[19], provide ecosystems services such as clean air[20] and water[21], and remain

57   strongholds for biological diversity[22-23]. As humans continue to encroach on these less-

58   influenced (i.e., "wilder"[7,14], "more ecologically intact"[19,22]) places, society increases the risk of

59   encounter with zoonotic-origin disease agents[24], such as the SARS-CoV-2 coronavirus. These

60   pathogens then trace back along the transportation networks embodied in the human footprint to

61   kill the vulnerable, weaken the healthy, and cause immense social and economic disruption[25].

62   Because so much depends on the human footprint, in practical and theoretical terms, it is

63   important that human footprint data be as accurate and frequently updated as possible. Past

64   efforts have been limited by temporal and spatial resolution of the underlying drivers[8,14,15,22].

65   The roads driver, for example, has been treated statically because there was only one map of

66   roads at the global scale[8]. All roads, from paths to superhighways, were given the same weight

67   because road types were undifferentiated. Population data were compiled in only five-year

68   increments and over unevenly sized units, the consequence of the different census geographies.

69   Similarly land cover/land use data were mapped inconsistently over time and using different

70   methods and sources across analyses. Related analyses leave out some components while adding

71   in others[26,27]. The combined effect has been to constrain the ability of scientists to systematically

72   measure change in human influence and fully understand its implications.

73   Here we present a 20-year annual retrospective taking advantage of higher spatial resolution,

74   more frequently updated, and better thematically resolved datasets, representing nine core drivers

75   of human influence to create the next-generation of human footprint maps (Figure 1a; Extended

76   Data Figures 1-3). We analyzed these data in two ways across all land areas except Antarctica

77   and adjacent Antarctic Islands using open-source methods. First, following in the tradition of the

78   "first-generation" of human footprint mapping[7,8], we used constant roads[28], rails[29], and

79   settlement[30] layers but combined them with higher-resolution, methodologically consistent,

80   dynamic population[31] and land cover[32] mapping to produce an annual time series of footprint

81   maps from 2000-2019 at nominal 300 m resolution. Second, we created new, "second-

82   generation" methods by supplementing these static data layers with dynamic, better defined

83   information about structures, roads, and railways data from the crowd-sourced Open Street

84   Map[33] (OSM) and replaced power consumption information, represented by stable night-time

85   lights data from the Defense Meteorological Satellite Program – Operational Linescan System[34]

86   (DMSP-OLS), with higher resolution, better calibrated night-time lights data from the Visible

87   Infrared Imaging Radiometer Suite[35] (VIIRS) for the period 2014 – 2019. By implementing our

88   analysis on the Google Earth Engine[36] and making the resulting maps, methods, and supporting

89   drivers freely available, we lower the barrier to future annual updates, enabling other researchers

90   to build on and improve our efforts.

91 Our study has broader implications than making sustainability research faster and more robust,

92 however. It quantitatively addresses the key question: How extreme are the impacts of human

93 actions on the natural environment? And how are these impacts varying over space and time in

94 the 21ˢᵗ century?

95 **Results**

96 *The quickening of human influence*

97 The primary metric of the human footprint is the human influence index (HII; see Methods,

98 Figure 1a, Table 1). The index maps a spatial gradient of human influence: from city centers,

99 through suburbs and exurban areas, to remote locales. Using the human footprint, one can

100 quantitatively describe areas as more or less artificial (influenced by human activity), or

101 conversely, less or more natural. "Human influence" in this sense represents both the degree to

102 which places have already been modified and the potential for on-going or future modification.

103 We note that the extremes of the human influence spectrum are theoretical, not real, constructs.

104 Even in places where the HII = 0, there remains human influence from climate change,

105 atmospheric deposition, or other global factors not captured in the index. Similarly even in the

106 most influenced places, such as midtown Manhattan, natural forces are in play: rain falls, winds

107 blow, soil accumulates, and plants and animals recruit, grow, reproduce, and die. Influence and

108 its converse, intactness, are relative concepts[7]. The improved resolution of the latest footprint

109 maps is such that one can observe these relative patterns at spatial scales from neighborhoods, to

110 nation states, to continents, to the world as a whole.

111 To demonstrate how HII is changing through time, we began by calculating the global mean HII

112 and assessing its variation (Figure 1b,c). Through analysis of the 2000 – 2019 time series of

113   human footprint maps using the first-generation methods, we observed that the mean global HII

114   score is relatively low (between 6 – 7 on a 0-60 scale) but increasing at an average rate of 0.33%

115   per year. We showed some years (2001, 2004, 2005, 2008) had modest global declines in mean

116   human impact against an overall increasing trend. These results correspond roughly to previous

117   analyses of human footprint change when studied with a non-continuous set of time points. For

118   example, Venter et al., observed a 9% increase in human influence from 1993 – 2009[8].

119   With the second-generation methods developed for this paper, including OSM and VIIRS

120   sources and appropriate weightings, we found that the global mean HII score was both higher

121   (mean 6.06 rather than 5.53, comparing first- to second-generation methods, on a 0 – 64 scale)

122   and accelerating six times faster than previously observed (average rate of 1.82% per year

123   compared to 0.27%; Figure 1b) from 2014 to 2019. The standard deviation in HII also widened

124   by nearly 25% over the study period on a global scale (Figure 1c). All drivers -- not only the

125   crowd-sourced ones from OSM -- grew in magnitude and extent, as described below, suggesting

126   that the acceleration of growth in mean HII is a broad-based phenomenon, driven by all inputs

127   (Figure 1d-e).

128   To place these rates of change in long-term perspective, we estimated the global mean HII over

129   the last 12,000 years using the Anthrome 12K dataset[37] (Methods; Extended Data Table 1).

130   Anthromes are “anthropogenically modified” land cover classes based on population density,

131   land use/land cover, and ecosystem type[38], using sources analogous to but more limited than our

132   inputs. Global estimates of mean HII extrapolated from anthromes (Figure 1f) grew on average

133   of 0.002% per year for the first 10,000 years of the Holocene; tripled its annualized rate of

134   growth to 0.006% in the first millennium of the Common Era; doubled again between 1000 –

135   1700, to 0.014%; grew almost an order of magnitude faster from 1700 – 1900, at 0.13%; and

136   nearly doubled again between 1900 – 2000, to grow at a rate of 0.25% per year. Temporal

137   patterns in the rates of change over the first fifteen years of the 21st century were similar for the

138   Anthrome 12K extrapolation and the first-generation human footprint analysis (Figure 1g). In

139   contrast, the second-generation human footprint, with temporally varying roads and improved

140   night-time lights, showed much faster growth in HII (Figure 1 g, analysis 3). The highest rate of

141   changed of mean HII in the study occurred from 2016 to 2017 (3.21% per annum). In summary,

142   our results suggest that human influence on Earth grew faster from 2014 - 2019 than at any

143   previous time in the last 12,000 years, and stood in 2019, before the SARS-CoV-2 pandemic, at

144   the greatest levels of influence, both in magnitude and extent, yet recorded in human history.

145   ***The relative importance of drivers of human influence***

146   To better understand these overall trends in human influence, we analyzed the contribution of

147   each of the nine drivers over time. Proportionally population density, land cover, and roads were

148   consistently the largest contributors to human influence globally, contributing on average,

149   31.1%, 30.4%, and 22.1% of mean HII, respectively, using the first-generation methods (Figure

150   1d). Because of past limitations with earlier human footprint mappings[7,8], variation in human

151   influence could only be driven by changes in population density, land cover, and/or power

152   consumption, since these are the only factors that varied. Population density and land cover

153   drivers increased on average 0.52% and 0.36% per year, respectively, from 2000 – 2019.

154   Although the nighttime lights/power driver contributed on average only 10.9% of total human

155   influence over this period, considerable inter-annual variation was observed, even after

156   radiometric calibration and other adjustments to compensate for blooming in the DMSP time

157   series[39]. Some years showed inter-annual increases in mean value (e.g. +5.3% from 2003 –

158   2004) while others had decreases (-4.9% from 2004 – 2005, -4.1 from 2005-2006). These

159   fluctuations may be due to changes in economic activity[40] and/or variability in the sensor output

160   that persist after correction and may be the reason why earlier studies of the human footprint[8],

161   and ours, observed reductions in human influence in some areas. Over the entire 2000 – 2019

162   period, however, the DMSP-derived, power driver, showed a net increase; on average, its global

163   mean score increased 0.92% per year in that time. The world is growing brighter at night.

164   Adding in the OSM and VIIRS data shifted the relative contributions of the different drivers in

165   the second-generation results (Figure 1e): proportionally, roads drove more of overall human

166   impacts, contributing 33.3% of mean global human influence, followed by population density

167   (27.2%), land cover (26.3%), power (5.9%), structures (2.9%), accessibility from coastal and

168   navigable waters (2.9%), and railways (1.6%).

169   The accelerating trend seen in the second-generation human footprint mapping is largely due to

170   adding the crowd-sourced OSM data, which have been improving in recent years[41,42]. The

171   increases could be the result of new construction of roads and infrastructure or increased

172   documentation of pre-existing roads and infrastructure as the OSM data has become complete. It

173   is impossible to entirely differentiate between these two cases given the existing OSM data

174   structure, which does not record the date of construction. It seems most plausible that both are

175   true: past efforts under-estimated human influence and human influence globally is continuing

176   to accumulate, but the exact timing is provisional.

177   The validation of HII scores against high-resolution aerial photography helped bring these

178   abstract measurements into focus by highlighting how quotidian changes in human footprint

179   have become in the 21st century: the felling of a forest for a field, the paving of a road, the

180   replacement of an open field with housing (see Methods; Extended Data Figure 3). Through

181   validation exercises, we verified that we mapped the presence or absence of human influence

182 with 98.9% overall accuracy. By driver, validation comparisons indicate that our maps reliably

183 showed the presence of verifiable roads, 98.0%, of cases; types of land use, 91.2%; built

184 structures (other than roads and railways), 69.4%; and access from navigable waters, 68.0%. We

185 also showed an inter-validator Kappa statistic of 0.8 (strong agreement between validators). For

186 all drivers, error rates of commission were less than error rates of omission, suggesting that our

187 footprint maps, while extraordinary, are in fact conservative treatments of change (Extended

188 Data Table 2).

189 *The loss of uninfluenced areas and intensification of human influence elsewhere*

190 To further characterize the spatial pattern of human influence change, we subtracted the 2019

191 and 2000 human footprint maps on a cell-by-cell basis (Figure 2a). This analysis revealed that

192 human impact index scores increased across 42.5% of the global land area (excluding Antarctica

193 and Antarctic Islands), decreased in 6.4% of the area, and did not change in the remaining 51.1%

194 (Figure 2b). Increases were clustered in North America (especially the United States), Europe,

195 the Arabian Peninsula, the Sahel, India, China, and Southeast Asia. Clusters of decreasing HII

196 were found in former industrial areas in the United States, Canada, Europe and Asia; in war torn

197 areas such as the Horn of Africa, Syria and Iraq; and in rural areas in proximity to growing urban

198 centers, such as coastal Central Africa, Turkey, Eastern Europe, and western Japan, for example.

199 Where decreases are observed, they were driven primarily by changes in the nighttime

200 lights/power driver in the first-generation methods from 2000 - 2014 (56% of countries), whereas

201 in the second-generation methods from 2014 – 2019, changes in land use drove most decreases

202 (62% of countries) (Extended Data Table 3). Despite pockets of decrease, we observed that all

203 countries of the world, with the exception of the Principality of Andorra (5% decrease), saw the

204   mean and sum of human impacts increase from 2000 to 2019 (Extended Data Table 4). The

205   Spratly Islands[43] in the South China Sea saw the greatest proportional increase, 749%.

206   Taking the difference of the frequency histograms of HII scores recorded for the 2000 and 2019

207   footprints revealed how much human influence have both expanded into new areas and

208   intensified in existing areas of influence (Figure 2c). The greatest decrease in frequency was

209   observed for previously uninfluenced areas (HII = 0), a loss of area of 3.07 million km^2 (Figure

210   3a,b), equivalent to about a third of the land area of the United States of America. Nearly all

211   uninfluenced areas have been erased from the temperate zone (e.g. Figure 3c); similarly major

212   portions of the Amazon Basin (Figure 3d) and central African forests, the Chang Tang region in

213   China, and even remote, arid regions in Australia (Figure 3e) and the Sahara Desert, have been

214   subjected to advancing human influence. Visibly, these patterns appear to be driven by the

215   extension of roads over the last two decades, followed by increased population density,

216   infrastructure, and associated power consumption.

217   The human footprint also intensified in areas subjected to some level of existing human

218   influence. We observed that the frequency of nearly all HII values greater than 1 increased, with

219   the greatest increases in the HII ranges 2 - 4, 7 – 9, 14 – 19, and 26 – 41 (Figure 2c). As HII is a

220   composite index there are multiple ways in which these intermediate values can be generated.

221   Based on visual inspection and the weighting of HII (Methods), we interpret increases in HII 2 –

222   4 values to be associated with the extension of access into peri-wilderness areas following new

223   (or newly mapped) roads; 7 – 9 with conversion of mosaic cropland / natural vegetation areas

224   through expanding agriculture; 14 – 19 with intensification of development in and around

225   existing croplands, and 26 – 41 with intensification of suburban and ex-urban development in the

226   United States, the Caribbean, Europe, India, northern China, and Java, and other regions with

227   proximity to existing towns and cities. Some reversals were noted in Eastern Europe, northeast

228   Asia, and the northeastern USA and southeastern Canada, which may be associated with

229   agricultural abandonment and rural depopulation, and in Somalia and Angola, in areas of social

230   unrest and conflict.

231   **Discussion**

232   *Policy implications*

233   The human footprint measures in some sense what was once called "civilization"[44], at least the

234   physical manifestations of it: the expansion of population; the construction of infrastructure and

235   settlements; the conversion of forests, grasslands, and wetlands to farms, fields, and cities; and

236   since the Industrial Revolution, the deployment of power beyond what muscle can supply.

237   Domesticating the Earth[18,37] has been an approximately 12,000-year project and brought many

238   benefits to humanity: a diverse populace nearing eight billion; declines in extreme poverty;

239   improvements in health and education; advances in arts, literature, science, and technology;

240   increased freedoms for some; modest wealth for many, and extraordinary wealth for a few[45].

241   However, the costs have also been enormous in terms of a changing climate, loss of biodiversity,

242   discombobulated ecosystems, and increased vulnerability to pandemic disease[2,5,14,25, 46]. Some

243   have lost more than they gained[47]. Yet all of us inhabit our shared world and pursue our

244   ambitions under the assumption that the planet will provide a safe and hospitable environment

245   into the future. That assumption is becoming increasingly less tenable[48]. What a terrible and

246   tragic irony it would be if we destroyed the underpinnings of our success by extending the

247   human footprint too far and too fast because we, the change makers, would not change what it

248   means to succeed.

249 Our fate is not fixed, however. Human influence is not inevitably negative impact[7]. The premise

250 and promise of sustainability science is that we can understand the effects we are having on the

251 planet and mitigate the less desirable ones, through planning, practice, and a commitment to use

252 what we learn. For society to shape the human footprint in manner consonant not only with the

253 needs of the current generation but for future generations as well, it is clear that more needs to be

254 done to shape the human footprint to provide for people and nature[5,46]. We draw out a few

255 implications here.

256 Clearly this analysis highlights that the road network deserves special attention[49,50]. Roads are

257 the vanguard of new development, the facilitator of transportation induced climate emissions,

258 and the conduit by which disease organisms move from safe harbors within intact ecosystems

259 into the globally connected, human population. Road management is key to any global

260 sustainability strategy. Closing roads that are no longer needed, especially in the more intact

261 parts of the world, is one of the easiest ways to slow the expansion of the human footprint[51].

262 Countries exist at different stages of development. Some undoubtedly need more infrastructure

263 to advance social and economic goals[52]. But all countries should consider the marginal benefits,

264 as well as the marginal costs, of extending the next highway, laying the next foundation, or

265 clearing the next wetland or forest patch for agriculture. Such decisions are not isolated, but

266 connected with past decisions and freighted with consequences for the future. Keeping equity

267 and justice in mind, we need to do as much as we can with the infrastructure we have, repairing

268 it where we must and removing it where no longer needed, before committing to the next

269 transformation of a world already so transformed.

270 Meanwhile the underlying drivers of the human footprint's drivers (population, land use,

271 infrastructure, and power consumption) are themselves in flux. It would be a mistake to interpret

272 the trends of the last two decades as predictions for the next twenty years. Long-term

273 demographic shifts are slowing the rate of population growth, even as the population continues

274 to grow[51]. Humanity continues to concentrate in towns and cities, with wide-reaching, socio-

275 ecological implications[8,45,52]. Some suggest we have already passed peak land conversion for

276 agriculture[53]. In fora around the world, advocates for more infrastructure and development are

277 increasingly pressed to answer: To what end? For whom? And at what cost?

278 The human footprint is a critical way to inform these discussions, assess their results, and when

279 coupled with other scientific models, articulate why they matter. A next-generation

280 sustainability science, building off a regularly and consistently updated human footprint, has

281 much to offer in guiding these historical phenomena toward successful socioeconomic pathways

282 where people and nature not only co-exist but thrive for generations yet to come.

283 **References**

284   1. Lewis, S. L. & Maslin, M. A. Defining the Anthropocene. *Nature* **519**, 171–180 (2015).

285   2. Di Marco, M., Venter, O., Possingham, H. P. & Watson, J. E. M. Changes in human

286   footprint drive changes in species extinction risk. *Nat. Commun.* **9**, 4621 (2018).

287   3. Grantham, H. S. et al. Anthropogenic modification of forests means only 40% of

288   remaining forests have high ecosystem integrity. *Nat. Commun.* **11**, 5978 (2020).

289   4. Ward, M. et al. Just ten percent of the global terrestrial protected area network is

290   structurally connected via intact land. *Nat. Commun.* **11**, 4563 (2020).

291   5. Masson-Delmotte, V. et al. *Climate Change 2021: The Physical Science Basis.*

292   *Contribution of Working Group I to the Sixth Assessment Report of the*

293   *Intergovernmental Panel on Climate Change*. (Cambridge University Press, 2021).

294   6. Córdoba-Aguilar, A., Ibarra-Cerdeña, C. N., Castro-Arellano, I. & Suzan, G. Tackling

295   zoonoses in a crowded world: Lessons to be learned from the COVID-19 pandemic. *Acta*

296   *Tropica* **214**, 105780 (2021).

297   7. Sanderson, E. W. et al. The human footprint and the last of the wild. *BioScience* **52**, 891–

298   904 (2002).

299   8. Venter, O. et al. Sixteen years of change in the global terrestrial human footprint and

300   implications for biodiversity conservation. *Nat. Commun.* **7**, 12558 (2016).

301   9. Watson, J. E. M. & Venter, O. Mapping the continuum of humanity's footprint on land.

302   *One Earth* **1**, 175–180 (2019).

303   10. Yackulic, C. B., Sanderson, E. W. & Uriarte, M. Anthropogenic and environmental

304   drivers of modern range loss in large mammals. *Proc. Natl. Aca. Sci. U.S.A.* **108**, 4024–

305   4029 (2011).

306   11. Macdonald, D. W. et al. Predicting biodiversity richness in rapidly changing landscapes:

307   climate, low human pressure or protection as salvation? *Biodivers. Conserv.* **29**, 4035–

308   4057 (2020).

309   12. Gallardo, B., Zieritz, A. & Aldridge, D. C. The Importance of the human footprint in

310   shaping the global distribution of terrestrial, freshwater and marine invaders. *PLOS ONE*

311   **10**, e0125801 (2015).

312   13. Falcão, J., Carvalheiro, L., Guevara, R. & Lira-Noriega, A. The risk of invasion by

313   angiosperms peaks at intermediate levels of human influence. *Bas. & Appl. Ecol.* **59**, 33-

314   43 (2021).

315   14. Williams, B. A. et al. Change in terrestrial human footprint drives continued loss of intact

316   ecosystems. *One Earth* **3**, 371–382 (2020).

15. Brennan, A. et al. Functional connectivity of the world's protected areas. *Science* **376**, 1101–1104 (2022).

16. Harper, A. B. et al. Land-use emissions play a critical role in land-based mitigation for Paris climate targets. *Nat. Commun.* **9**, 2938 (2018).

17. Lamb, W. F. et al. A review of trends and drivers of greenhouse gas emissions by sector from 1990 to 2018. *Environ. Res. Lett.* **16**, 073005 (2021).

18. Kareiva, P., Watts, S., McDonald, R. & Boucher, T. Domesticated nature: Shaping landscapes and ecosystems for human welfare. *Science* **316**, 1866–1869 (2007).

19. Watson, J. E. M. et al. The exceptional value of intact forest ecosystems. *Nat. Ecol. Evol.* **2**, 599–610 (2018).

20. Butt, E. W. et al. Large air quality and human health impacts due to Amazon forest and vegetation fires. *Environ. Res. Commun.* **2**, 095001 (2020).

21. Harrison, I. J. et al. Protected areas and freshwater provisioning: a global assessment of freshwater provision, threats and management strategies to support human water security. *Aqua. Cons.: Mar. & Freshw. Ecos.* **26**, 103–120 (2016).

22. Betts, M. G. et al. Global forest loss disproportionately erodes biodiversity in intact landscapes. *Nature 547*, 441–444 (2017).

23. Allan, J. R. et al. The minimum land area requiring conservation attention to safeguard biodiversity. *Science* 376, 1094–1101 (2022).

24. Allen, T. et al. Global hotspots and correlates of emerging zoonotic diseases. *Nat. Commun.* **8**, 1124 (2017).

25. Dobson, A. P. et al. Ecology and economics for pandemic prevention. *Science* **369**, 379–381 (2020).

26. Kennedy, C. M., Oakleaf, J. R., Theobald, D. M., Baruch-Mordo, S. & Kiesecker, J. Managing the middle: A shift in conservation priorities based on the global human modification gradient. *Global Change Biology* **25**, 811–826 (2019).

27. Theobald, D. M. et al. Earth transformed: detailed mapping of global human modification from 1990 to 2017. *Earth System Science Data* **12**, 1953–1972 (2020).

28. Center for International Earth Science Information Network - CIESIN - Columbia University & Information Technology Outreach Services - ITOS - University of Georgia. *Global Roads Open Access Data Set, Version 1 (gROADSv1).* https://sedac.ciesin.columbia.edu/data/set/groads-global-roads-open-access-v1 (2013).

29. United States National Imagery and Mapping Agency. *Vector Map Level 0 (VMAP0).* (2000).

30. Corbane, C. et al. Automated global delineation of human settlements from 40 years of Landsat satellite data archives. *Big Earth Data* **3**, 140–169 (2019).

31. Tatem, A. J. WorldPop, open data for spatial demography. *Sci Data* **4**, 170004 (2017).

32. European Space Agency. *Land Cover CCI Product User Guide Version 2. Tech. Rep.* https://www.esa-landcover-cci.org/?q=node/175 (2017).

33. OpenStreetMap Wiki contributors. *Main Page.* https://wiki.openstreetmap.org/wiki/Main_Page (2020).

34. Imhoff, M., Lawrence, W. T., Stutzer, D. C. & Elvidge, C. D. A technique for using composite DMSP/OLS "City Lights" satellite data to map urban area. *Rem. Sens. of Environ.* **61**, 361–370 (1997).

35. Elvidge, C. D., Baugh, K., Zhizhin, M., Hsu, F. C. & Ghosh, T. VIIRS night-time lights. *Int. J. of Rem. Sens.* **38**, 5860–5879 (2017).

363   36. Gorelick, N. et al. Google Earth Engine: Planetary-scale geospatial analysis for everyone.

364   *Rem. Sens. of Environ.* **202**, 18–27 (2017).

365   37. Ellis, E. C., Beusen, A. H. W. & Goldewijk, K. K. Anthropogenic Biomes: 10,000 BCE

366   to 2015 CE. *Land* **9**, 129 (2020).

367   38. Ellis, E. C., Klein Goldewijk, K., Siebert, S., Lightman, D. & Ramankutty, N.

368   Anthropogenic transformation of the biomes, 1700 to 2000: Anthropogenic

369   transformation of the biomes. *Glob. Ecol. and Biogr.* **19**, 589–606 (2010).

370   39. Li, X., Zhou, Y., Zhao, M. & Zhao, X. A harmonized global nighttime light dataset

371   1992–2018. *Sci Data* **7**, 168 (2020).

372   40. Chen, X. & Nordhaus, W. D. Using luminosity data as a proxy for economic statistics.

373   *Proc. Natl. Aca. Sci. U.S.A.* **108**, 8589–8594 (2011).

374   41. Herfort, B., Lautenbach, S., Porto de Albuquerque, J., Anderson, J. & Zipf, A. The

375   evolution of humanitarian mapping within the OpenStreetMap community. *Sci Rep* **11**,

376   3037 (2021).

377   42. Barrington-Leigh, C. & Millard-Ball, A. The world's user-generated road map is more

378   than 80% complete. *PLOS ONE* **12**, e0180698 (2017).

379   43. Specia, M. & Takkunen, M. South China Sea photos suggest a military building spree by

380   Beijing. *The New York Times*. February 8 (2018).

381   44. Braudel, P. F. *Afterthoughts on Material Civilization and Capitalism*. (The Johns

382   Hopkins University Press, 1977).

383   45. Sanderson, E. W., Walston, J. & Robinson, J. G. From bottleneck to breakthrough:

384   Urbanization and the future of biodiversity conservation. *BioScience* **68**, 412–426 (2018).

385   46. Brondizio, E.S., Settlele, J., Diaz, S., & Ngo, H.T (eds). *Global assessment report of the*

386   *Intergovernmental Science-Policy Platform on Biodiversity and Ecosystem Services.*

387   (IPBES Secretariat, 2019).

388   47. McNeill, J. R. *Something New Under the Sun: An Environmental History of the*

389   *Twentieth-Century World.* (W. W. Norton & Company, 2001).

390   48. Steffen, W. et al. Planetary boundaries: Guiding human development on a changing

391   planet. *Science* **347**, 1259855 (2015).

392   49. Laurance, W. et al. A global strategy for road building. *Nature* **514**, 262–262 (2014).

393   50. van der Marel, R. C., Holroyd, P. C. & Duinker, P. N. Managing human footprint to

394   achieve large-landscape conservation outcomes: Establishing density limits on motorized

395   route-user networks in Alberta's Eastern Slopes. *Glob. Ecol. Cons.* **22**, e00901 (2020).

396   51. Bicknell, J., Gaveau, D., Davies, Z. & Struebig, M. Saving logged tropical forests:

397   Closing roads will bring immediate benefits: peer-reviewed letter. *Fron. Ecol. Envi.* **13**,

398   73–74 (2015).

399   52. Rozenberg, J. & Fay, M. Beyond the Gap: How Countries Can Afford the Infrastructure

400   They Need while Protecting the Planet. (World Bank, 2019).

401   53. Lutz, W. & Qiang, R. Determinants of human population growth. *Phil. Trans. Roy. Soc.*

402   *London. Series B: Biol. Sci.* 357, 1197–1210 (2002).

403   54. Dyson, T. The role of the demographic transition in the process of urbanization. *Pop.*

404   *Dev. Rev.* **37**, 34–54 (2011).

405   55. Ausubel, J. H., Wernick, I. K. & Waggoner, P. E. Peak Farmland and the Prospect for

406   Land Sparing. *Pop. Dev. Rev.* **38**, 221–242 (2013).

407

Methods

Overview

Building on previous studies[7,8,14, 26, 27], we studied five broad categories of human impact on nature (Table 1): population density, land cover/land use, built infrastructure, accessibility, and power consumption. Clearly, these drivers do not reflect all ways that human beings influence the environment nor do they reflect the impact of each person equally. Our claims, based on the extensive supporting literature[2-4,9,11-14,18-25] (see also: Supplemental Materials) are more modest: that when these factors exist in the landscape, some species, especially non-human commensal species, and ecosystem qualities such as vegetative cover, permeability, and species richness and abundance are more likely influenced by human activity than areas in a less or uninfluenced state[46]. Moreover, when these drivers co-occur, or more intensive forms of the drivers are present, the cumulative influence, and likely impacts, are also greater.[9,19]

Because higher resolution, more complete datasets became available only for later years of our study period, we studied the human footprint in two, overlapping time series. As detailed in the main text, the traditional "first-generation methods" deploy temporally-varying population, land cover, and power consumption / nighttime lights data and static representations of waterways, roads, railways, and infrastructure. The "second-generation" methods use these same types, but supplemented with temporally varying, better resolved and tagged data on roads, railways, waterways, and infrastructure, and higher resolution, better calibrated nighttime lights data. These improvements enable us to detect change more accurately and at higher resolution spatial and temporal resolution that previous analyses[8,16,27].

429   All driver data, regardless of native spatial resolution, were analyzed within Google Earth

430   Engine[36] using the same system of 3-arc-second cells, which have a nominal 300-meter square

431   side at the Equator. Google Earth Engine measures areas on a per-cell basis, so areas reported

432   here account for variation in cell size with latitude.

433   To facilitate comparison, we weighted each driver on a 0 – 10 scale, so that a value in one driver

434   is roughly comparable to the same value in another driver. We then summed over the drivers as

435   to arrive at the Human Impact Index (HII), which we measured to two decimal places (0.00) and

436   stored as integers by multiplying by 100. Where possible we used methods similar to earlier

437   studies to enable long-term comparability[7-9,14]. We plotted human footprint maps for 2009

438   between this study resampled to match Venter et al.[8] 2009 footprint to show close agreement

439   between the two analyses (Extended Data Figure 5).

440   *Population density*

441   People, like all other species, interact with organisms and ecosystems where they live. These

442   interactions are density-dependent to some extent, especially at low levels of human population

443   density[19,26]. Density-dependent impacts include noise, pollution, hunting, gathering, vegetation

444   stomping and removal, disturbance of wildlife, and other such factors.

445   For both time series, we used the WorldPop Unconstrained Residential Population dataset[31],

446   which disaggregates administrative unit population counts from national and subnational

447   censuses into grid cell-based counts on an annual basis, using other geospatial datasets and

448   Random Forest machine learning techniques[56].

449   Following Venter et al.[8], to represent the impacts from human population density, we gave any

450   cell with a density greater than 1000 people per square km a weight of 10. For less densely

451   inhabited areas, we applied the logarithmic scaling function shown in Table 1.

452   ***Land cover***

453   Human beings impact the environment through wholescale or partial transformation of

454   ecosystems associated with urbanization, agriculture, natural resource extraction, and animal

455   husbandry, with a wide variety of associated changes in species habitat and ecosystem

456   function.[46]

457   For both time series, we used the ESA CCI Land Cover Dataset[32], which provides 33 land cover

458   classes in an annual time series using a consistent methodology. We gave urban land cover a

459   weight of 10; irrigated croplands, 8; rainfed croplands, 7; and mosaic cropland / natural

460   vegetation with population densities greater than or equal to 1 person per square km received a 6

461   when cropland was more than 50% of the area, and a 4 when cropland was less than 50%. All

462   other classes (e.g. tree-covered areas, grasslands, shrublands, sparsely vegetated classes, lichens

463   and mosses) received a weight of 0 (see Supplementary Information Figure S1).

464   *Built infrastructure*

465   Human beings modify the landscape with built structures, which displace the existing

466   ecosystems, disrupting habitats, altering water movements and air flows, changing the thermal

467   environment, arresting soil development, and providing barriers to movement.[46] Energy

468   expended in and by using infrastructure contributes to climate change.[5,17] We considered three

469   categories of built infrastructure: roads, railways, and a wide-array of other built infrastructure.

470   (Supplementary Information Figure S2-S4).

471   Built infrastructure is critical to many social, economic, humanitarian, and environmental

472   analyses that it is surprising that globally consistent, publicly available datasets have been

473   lacking for so long. In the first-generation time series we mapped roads using static methods

474   comparable with past efforts, using gRoads[28], VMap0[29], and Global Human Settlement Layer[30,57]

475   datasets (Table 1.)

476   To supplement these static data with dynamic data in the second-generation methods, we

477   automated ingestion of Open Street Map[33] (OSM) data into Google Earth Engine. Volunteer

478   mappers and organizations continuously create and maintain the OSM data. We fetch the OSM

479   Protocolbuffer Binary Format file, convert it to a text file using the Osmium C++ library[58], then

480   split that file into individual files for each tag pertaining to roads, railways, and infrastructure,

481   discarding invalid and infinitesimal geometries. Linear and point features are rasterized using the

482   GDAL library[59], where each 300 m cell for each tag is assigned a value of 1 if any feature with

483   the specified tag is present. We update the previous time point then ingest the data into Earth

484   Engine as a single, multi-band image for the requested date, where each band represents an OSM

485   tag.

486   We weighted the direct impacts of infrastructure based on typologies identified in the source data

487   (Table 1; Supplementary Information Figures S2-S4). Paved major highways with more than

488   two lanes received a 10; paved, two lane, arterial roads received an 8; other roads, including

489   unpaved roads, paths and trails, received a 4. Railways received weights from 4 – 8 depending

490   on their operational status and/or type. Other structures received a weight of 10 for major

491   developments (e.g. housing developments, parking lots, airfields, landfills, quarries, nuclear

492   explosion site, etc.); an 8 for medium-sized clusters of development intermixed with vegetation

493   (e.g. residential houses, power lines, farm buildings, military bases, etc.); a 6 for scattered

494   developments (e.g. barns, isolated cabins, vegetated embankments, etc.); and other minor

495   developments of a limited scale received a 4 (e.g. ditch, snow fence, hut, zip line, etc.).

496   *Accessibility*

497   People have impacts beyond the places where they live, assuming they can get there[49]. Impacts

498   are similar to the ones described under population density, though generally less frequent,

499   therefore deserving of less weight.

500   We modeled accessibility using the simple declining exponential function based on distance

501   from roads and navigable waterways developed by Venter et al.[8] (Table 1). Open surface water

502   data were derived from analysis of radar and optical remote sensing data[60]. Waterways were

503   assumed to be navigable if they were at least 300 m wide in one dimension, including coasts.

504   We assumed all roads are accessible, as well as waterways within 15 km of a population center

505   (defined as a cell with population density of 10 or more people per square km). We gave access

506   points from water a weight of 4, or for roads, half of direct impact (4, 4, or 2, depending on type;

507   Supplementary Information Figure S4), at the point of access, declining to 0 beyond 15 km. We

508   did not give railways an indirect weight.

509   *Power*

510   We included a proxy for power utilization because the ability to harness energy to do work

511   greatly amplifies the ability of human beings to alter the environment. One person with an eight

512   ton, diesel-fueled bulldozer can create changes to the environment much faster and more deeply

513   than that same person with a shovel because more energy is expended in the same period of time

514   and physical limitations of bone and muscle are removed. The same applies for other kinds of

515   machinery: cars, trucks, lawn mowers, leaf blowers, etc. We assume the ability to access power

23

516   from electricity or fossil fuels follows the pattern of stable night-time lights measured by

517   satellites. Artificial light during the nighttime hours can also have a disruptive effect on

518   wildlife[61,62] in addition to being a proxy for human uses of non-muscle power. Nighttime lights

519   are also approximate measures of economic activity[40,63].

520   We used datasets from two satellite platforms to measure nighttime lights: the Defense

521   Meteorological Satellite Program/Operational Linescan System[34] (DMSP) and the Visible

522   Infrared Imaging Radiometer Suite[35] (VIIRS) mounted on the Suomi NPP satellite mission. The

523   VIIRS sensor is four times better resolved than the DMSP data (15 arc-seconds rather than 30

524   arc-seconds), performs an on-board calibration, is both more sensitive in low-light conditions

525   and less subject to saturation in high light areas than DMSP, and is offered in monthly time

526   rather than annual time series. However the VIIRS data is only available since 2014. First-

527   generation human footprint methods use the DMSP data to present power consumption; the

528   second-generation methods, the VIIRS data. We developed an inter-calibrated, largely

529   comparable mapping by adapting the procedures suggested by Li et al.[38]. That method creates

530   annual composites of the VIIRS data, controls for noise using a min-max stretch that varies by

531   latitude, and then converts VIIRS radiance values into a 0-63 Digital Number scale comparable

532   to DMSP. It also inter-calibrates across the different DMSP sensors, including recently available

533   data that carry the DMSP time series through 2019.

534   To weight the lights data, we analyzed the deciles of the frequency distribution of pixels for the

535   first year in the time series, using the methods from Venter et al.[8]. Weights of $0 - 10$ were

536   applied to the 10 decile ranges (Supplementary Information Figure S5). The same ranges were

537   used for all time points to maintain comparability.

538   *Validation*

539   To validate our human impact mapping, we randomly selected 2521 cells stratified by level of

540   development: high (HII > 46.66), medium (HII 23.33 – 46.65) and low levels (HII 0 – 23.32) of

541   impact and within 6 bands of 60 degrees of longitude each, to ensure geographic coverage. For

542   each cell, we further randomly selected three years between 2000 - 2019. We examined high-

543   resolution aerial imagery in Google Earth Pro by overlaying the cell boundaries on the imagery

544   and taking advantage of the "historical imagery" feature, choosing the closest date of available

545   imagery within twelve months of the randomly selected year. We scored cloud-free, clear

546   images for visible signs of built infrastructure, land cover type, the presence of roads, and

547   navigable waters, using the same scoring rubric applied to the driver data, and dropping locations

548   where imagery was unavailable or unclear. If there were no roads or navigable waters within the

549   cell boundaries, we measured the distance from the center of the cell to the nearest visible road

550   or navigable waterway, up to 15 km. We did not score for population density or power (e.g.

551   nighttime lights) since population density was not directly observable and the imagery was

552   collected in the daytime. We also do not report railway scores because we had too few samples

553   had railways to make the validation meaningful. Since identification to type was not always

554   possible visibly, we developed confusion matrices[64] for the presence or absence of signs of

555   human impact (HII) and of each driver (except population, nighttime lights, and railways)

556   individually. From these matrices, we calculated rates of overall accuracy and errors of

557   commission and omission for 1,575 cells, using first-generation method footprints between 2000

558   – 2014, and second-generation footprints for 2015 – 2019. As further validation, two examiners

559   independently validated the same 15% of sample of the validation locations. We calculated

560   Cohen's Kappa Statistic to measure score reliability between validators[65].

561   *Anthrome 12K Analysis*

562   For each of classes in the 2015 Anthrome 12K map[37], we calculated the mean HII using the

563   second-generation human footprint for 2015 (Extended Data Table 2). We substituted class

564   means of HII in the 5 arc-minute, anthrome maps by class and calculated the global mean of

565   human impact for each time point. This analysis and the following three were conducted in

566   ArcGIS[66] version 10.7.1. All other calculations (including all calculations of area) were made

567   with Google Earth Engine[36].

568   *Driver Analysis*

569   For each driver for each time point, we calculated the mean and standard deviation, to estimate

570   the contribution to total HII.

571   *Country Analysis*

572   We used the GADM[67] version 3.6 level 0 boundaries to define countries with internationally

573   recognized ISO 3166-1 codes. We calculated the mean, sum, and standard deviation of HII for

574   each time point.

575   *HII Decrease Analysis*

576   On a per-cell basis we calculated the regression line through the HII values for 2000 – 2014

577   (first-generation methods) and 2015 – 2019 (second-generation methods) to find the cells that

578   decreased in HII by at least 0.25 / year. We analyzed these cells to find the driver whose

579   changes were most frequently associated with declines in HII on a country-by-country basis

580   using the GADM[67] version 3.6 level 0 boundaries.

581   *Unimpacted areas Analysis*

582 For purposes of this paper, we define unimpacted areas as cells where HII = 0. Such areas have,

583 by definition, zero population density, evince natural land cover types, have no built

584 infrastructure, are the equivalent of being more than 15 km from the nearest road or navigable

585 waterway, and emit no night-time lights, as mapped with the driver datasets described above.

586 We tallied unimpacted areas for the 2000 first-generation human footprint and the 2019 second-

587 generation footprint maps to estimate loss of such areas globally.

588 **Data availability**

589 All calculation outputs are available as Earth Engine Image assets with a consistent naming

590 convention based on the date for which the calculation was run. Human Impact Index images are

591 stored in the `projects/HII/v1/hii` ImageCollection (e.g. `projects/HII/v1/hii/hii_2001-01-01`).

592 Driver ImageCollections are also available to analysts with Earth Engine access to use

593 individually and combine in different ways: `projects/HII/v1/driver/infrastructure`,

594 `projects/HII/v1/driver/land_use`, `projects/HII/v1/driver/population_density`,

595 `projects/HII/v1/driver/power`, `projects/HII/v1/driver/railways`, `projects/HII/v1/driver/roads`,

596 and `projects/HII/v1/driver/water`.

597 For convenience, final HII datasets are also available as Cloud-Optimized Geotiffs, which can be

598 used in a desktop GIS via remote url or by downloading, with urls of the form

599 `https://storage.googleapis.com/hii-export/2001-01-01/hii_2001-01-01.tif`.

600 [Note to editor: All asset and tiff locations will be updated on `https://wcshumanfootprint.org`

601 prior to publication along with a user-friendly visualization application.]

602 **Code Availability**

We have made our open-source code available at

`https://github.com/SpeciesConservationLandscapes`. Each repository contains an explanatory

README as well as the Google Earth Engine code used to run the calculations. The computer

code is distributed under the GNU General Public License 3.0

(https://www.gnu.org/licenses/gpl-3.0.html).

Methods-only references

56. Stevens, F. R., Gaughan, A. E., Linard, C. & Tatem, A. J. Disaggregating Census Data

    for Population Mapping Using Random Forests with Remotely-Sensed and Ancillary

    Data. *PLOS ONE* **10**, e0107042 (2015).

57. Joint Research Centre (JRC), European Commission, & Center for International Earth

    Science Information Network (CIESIN). *Documentation for the Global Human*

    Settlement Layers (GHSL): Population and Built-Up Estimates, and Degree of

    Urbanization Settlement Model Grid. (NASA Socioeconomic Data and Applications

    Center, 2021).

58. Topf, J. *Osmium Library.* (2021). https://osmcode.org/libosmium/

59. GDAL/OGR contributors. *GDAL/OGR Geospatial Data Abstraction Software Library.*

    (Open Source Geospatial Foundation., 2021). doi:10.5281/zenodo.5884351.

60. Lamarche, C. et al. Compilation and Validation of SAR and Optical Data Products for a

    Complete and Global Map of Inland/Ocean Water Tailored to the Climate Modeling

    Community. *Rem. Sens.* **9**, 36 (2017).

61. Buxton, R. T. et al. The relationship between anthropogenic light and noise in U.S.

    national parks. *Land. Ecol* **35**, 1371–1384 (2020).

625 62. Schirmer, A. E. et al. Mapping behaviorally relevant light pollution levels to improve

626   urban habitat planning. *Sci. Rep.* **9**, 11925 (2019).

627 63. Gibson, J., Olivia, S., Boe-Gibson, G. & Li, C. Which night lights data should we use in

628   economics, and where? *J. Dev. Econ.* **149**, 102602 (2021).

629 64. Fernandez-Carrillo, A., Franco-Nieto, A., Pinto-Bañuls, E., Basarte-Mena, M. & Revilla-

630   Romero, B. Designing a Validation Protocol for Remote Sensing Based Operational

631   Forest Masks Applications. Comparison of Products Across Europe. *Rem. Sens.* **12**, 3159

632   (2020).

633 65. McHugh, M. L. Interrater reliability: the kappa statistic. *Biochem Med (Zagreb)* **22**, 276–

634   282 (2012).

635 66. Environmental Systems Research Institute (2021) *ArcGIS Desktop Software*.

636   http://esri.com

637 67. GADM contributors. *GADM maps and data.* https://gadm.org/about.html (2021).

638

639

640 **Acknowledgements**

643 **Competing Interests**

644 The authors declare no competing interests.

645 The authors and their institutions remain neutral with regard to jurisdictional claims in published

646 maps.

647
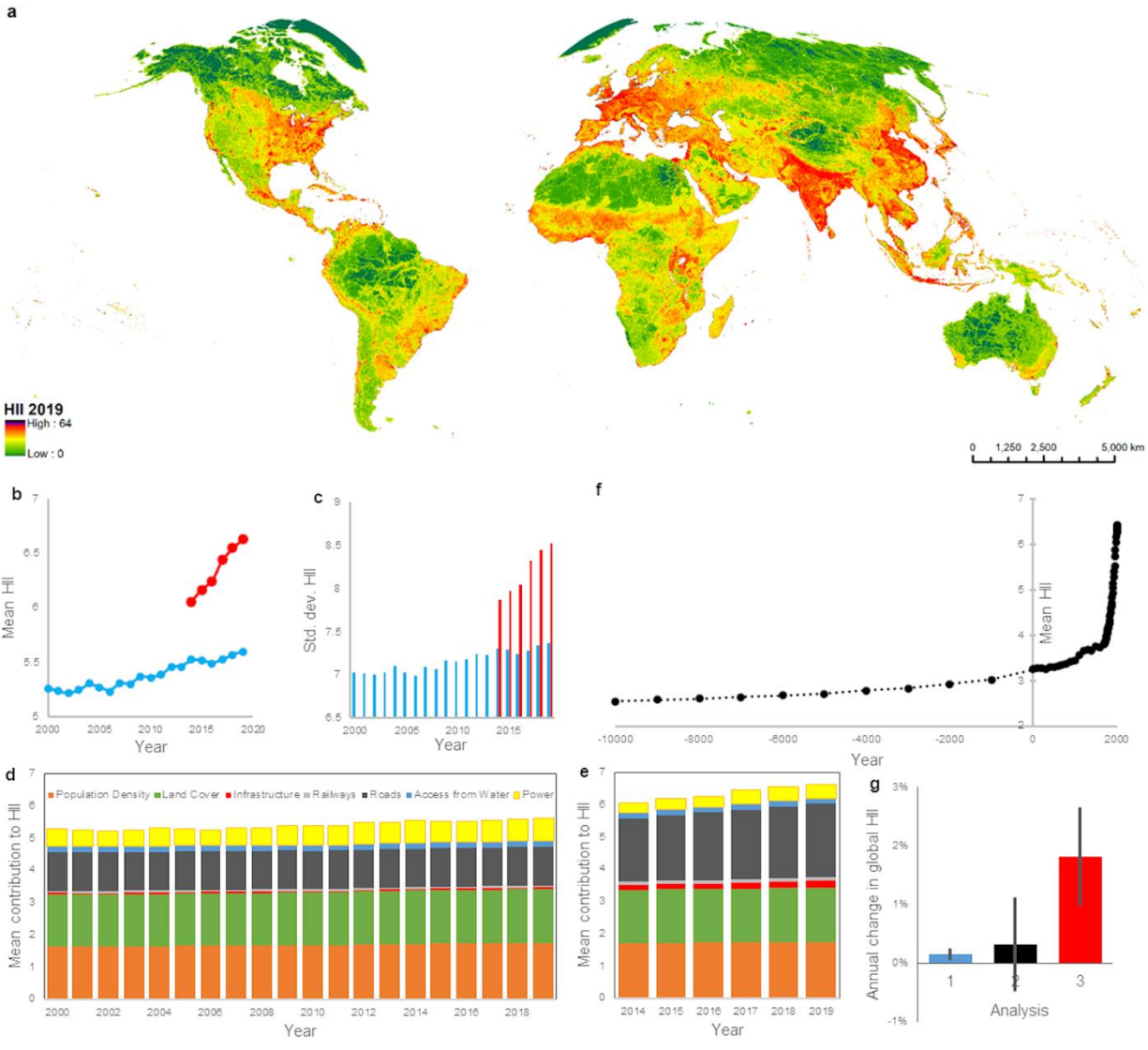
Figure 1. (a) The global map of the extent and intensity of the human impact index[7-9]

(colloquially the human footprint) on the land's surface (Antarctica excluded) in 2019. Red

colors represent relatively higher human impacts, green areas relatively lower. Human impact is

mapped at a nominal 300 m resolution. Detail maps and more color-blind friendly color schemes

are shown in the Extended Data. (b) Global mean of the human impact index (HII) from 2000 –

2019, using traditional, first generation methods, consistent with previous human footprint

maps[7,8], including static roads and infrastructure drivers but dynamic population, land use and

656   power consumption (blue) and improved, second generation methods, which include

657   dynamically changing roads and infrastrcuture and higher resolution nighttime lights (red); see

658   Main text. (c) Standard deviation of the HII, 2000 – 2019; first generation methods (blue),

659   second generation methods (red). (d) Mean contributions of five drivers of human impact

660   (population density, land cover, structures, railways, roads, access population centers along

661   navigable waters, and power consumption) to the human footprint, annually 2000 – 2019, using

662   first generation methods. (e) Mean contributions of the same drivers as (Figure 1d) annually

663   from 2014 – 2019, using second generation methods. (f) Extrapolated mean HII over the last

664   12,000 years extrapolated from the the Anthrome 12K analysis[36]. (g) Mean and standard

665   deviation of annual percentage change in mean HII for (1) first generation methods from 2000 –

666   2015, (2) the Anthrome 12K extrapolation from 2000 – 2015, and (3) the second generation

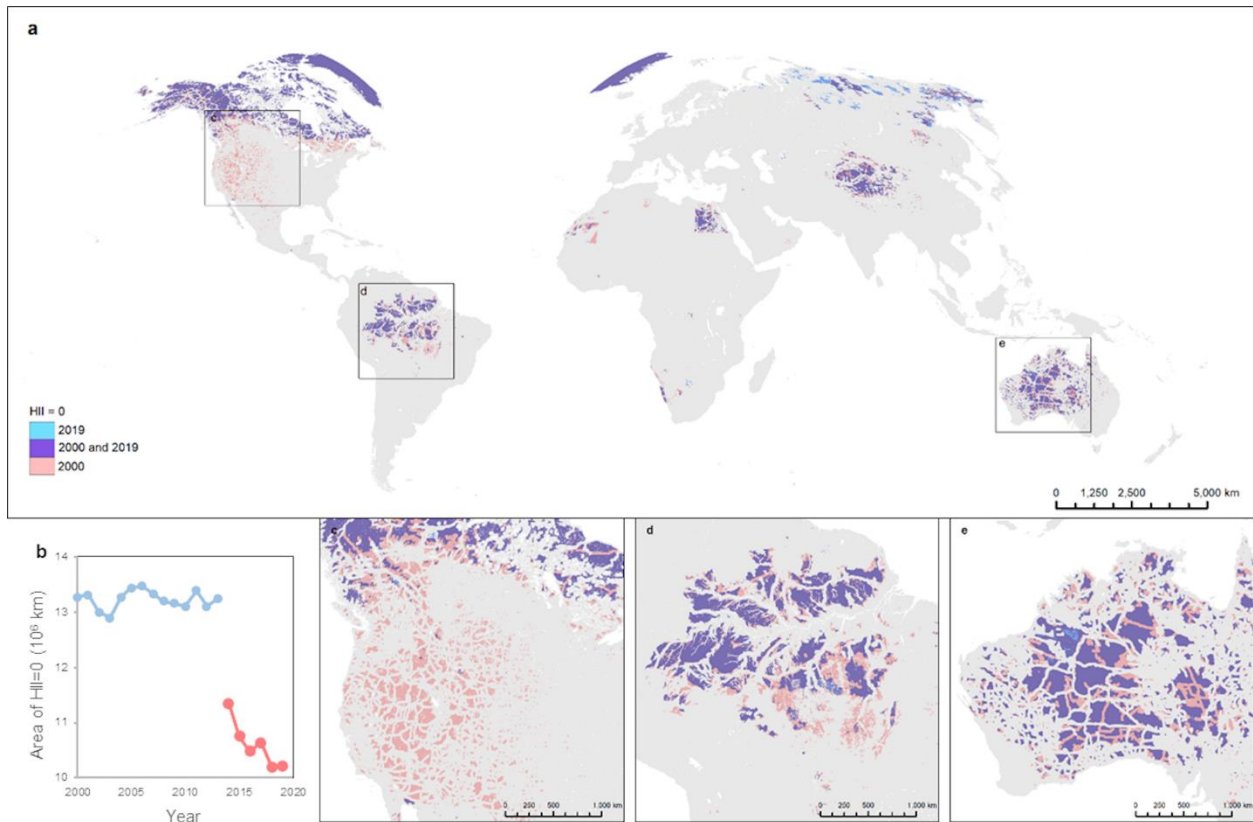667   methods from 2014 – 2019. See Main text for details.

668

669
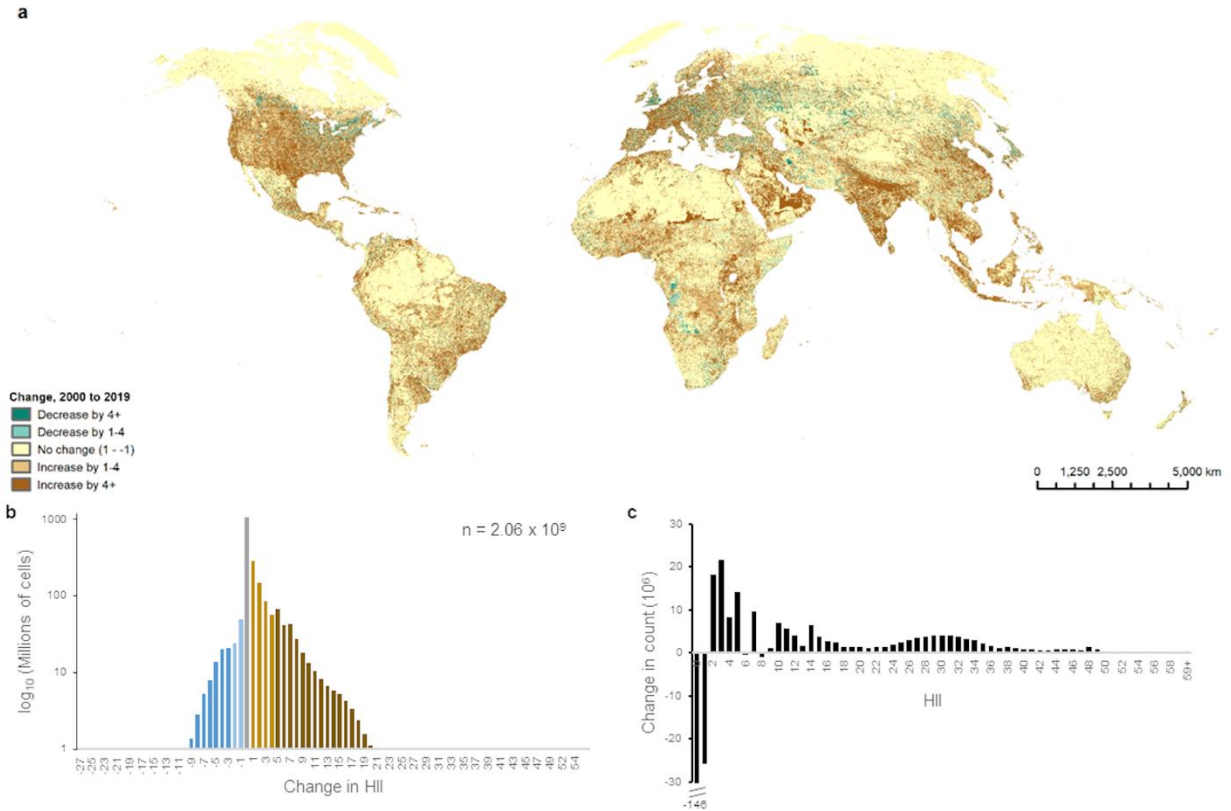
Figure 2. (a) Per-pixel change in human impact index (HII) between 2000 – 2019. (b)

Distribution of the magnitude of change in HII, 2000 – 2019. Note the logarithmic y-axis. n is

the total count of cells globally. (c) Change in frequency at each level of HII, comparing

histograms from 2000 and 2019.

674

675

676

Figure 3. (a) Map of unimpacted areas in 2000 (blue), 2019 (pink), and jointly (purple), as

measured by the human impact index (HII). Squares indicate locations of inset views. (b)

Change in the area of HII = 0 from 2000 – 2019 in millions of square km. The blue line

represents the trend in the first-generation human footprint analysis from 2000 – 2014; the red

line indicates second-generation human footprint trend from 2014 – 2019, after the inclusion of

dynamically changing roads and infrastructure data and improved nighttime lights. (c) Inset

view of western North America, (d) Inset view of the the Amazon Basin. (e) Inset view of central

and western Australia.

685

686 Table 1. Source and weightings of the nine drivers of human impact, 2000– 2019, using the first-
687 (2000 – 2019) and second-generation (2014 – 2019) methods.

Impact driver	First gene-ration.	Second gene-ration.	Global dataset	Native time period; frequency	Native resolution	Human impact weighting[a]
Population density	√	√	WorldPop[29] Residential Population	2000 – present; annual	100 m	3.333 * log(persons / km^2 + 1); if density > 1000 persons / km^2 → 10
Land Cover	√	√	ESA CCI Land Cover Dataset[30]	1992 – present; annual	300 m	Depends on land cover class and population density; 33 classes[a]
Infrastructure						
… Structures	√	√	Global Human Settlement Layer[28]	2000 – 2014; static	30 m	10
		√	Open Street Map[31]	2012 – present; weekly	Vector	Depends on type; 192 types[a]
… Roads	√	√	gRoads[26]	1980 – 2010; static	Vector	8
		√	Open Street Map[31]	2012 – present; weekly	Vector	Depends on type; 29 types[a]
… Railways	√	√	Vector Map 0[27]	c. 1990 – 2000; static	Vector	Depends on status; 5 classes[a]
		√	Open Street Map[31]	2012 – present; weekly	Vector	Depends on type; 14 types[a]
Accessibility						
… via Populated Coasts	√	√	ESA CCI Water Bodies Map[51]	2000; static	150 m	e^(distance * -0.0003) * 4[b]
… via Navigable Waters	√	√	Global Surface Waters[51]	1984 – present; annual	30 m	e^(distance * -0.0003) * 4[b]
… via Roads	√	√	gRoads[26]	1980 – 2010; static	Vector	e^(distance * -0.0003) * 4[c]
		√	Open Street Map[31]	2012 – present; weekly	Vector	e^(distance * constant) * weight[c]
Power	√		Inter-calibrated stable nighttime lights series from DMSP[32,38]	1992 – 2019; annual	30 arc-seconds	10 equal area quantiles[d] → 0 - 10
		√	Inter-calibrated stable nighttime lights series from VIIRS[33, 38]	2014 – present; annual	15 arc-seconds	10 equal area quantiles[d] → 0 - 10

688 a, Weightings vary from 0 – 10 and follow Venter et al.[8], except as noted. Weights are detailed in the Supplementary Information for each type and

689 class. Figure S1 shows land cover weights, Figure S2 built structure weights, Figure S3 road weights, Figure S4 railway weights, and Figure S5

690 power/night-time light weights.

691 b, Distance (km) from population center (defined by density > 10 persons / km^2) on coast or adjacent to navigable waterways up to 15 km.

692 c, Distance (km) from road up to 15 km; road constants and weights depend on the type of road; see Supplementary Information.

693 d. Mapping of quantiles is based on analysis of first year of time series and applied consistently to other time points, see Supplementary Information.

Extended data figures and tables
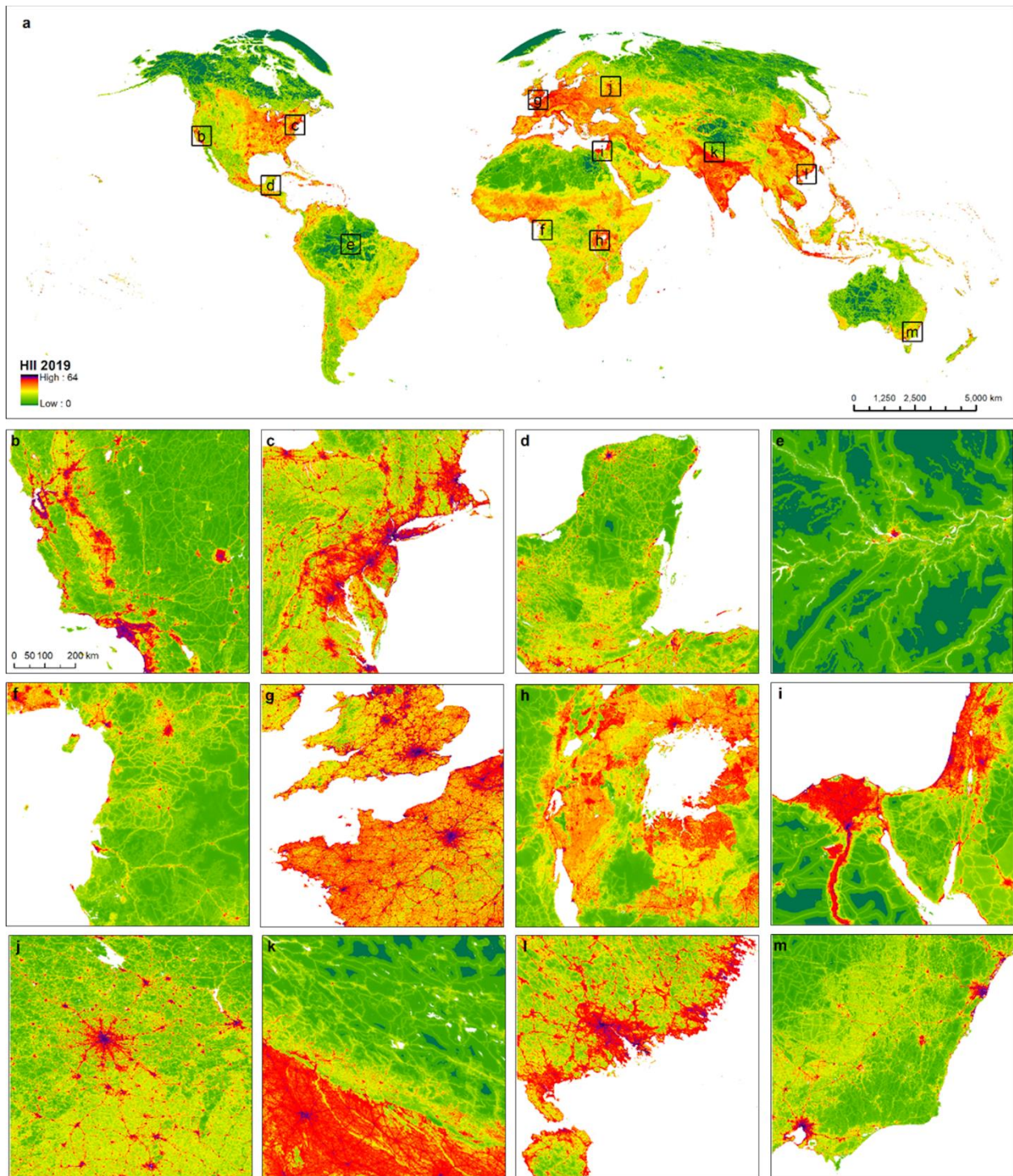
695

696   Extended Data Fig. 1. (a) Locations of detail views of the 2019 human footprint, illustrating (b)

697   central California, (c) the Northeast Corridor from Massachusetts to Virginia, (d) the Yucatan

698   Peninsula, (e) the central Amazon Forest around Manaus, Brazil, (f) parts of Nigeria, Cameroon,

699   and Gabon along the Gulf of Guinea, (g) southern England, northern France, and portions of

700   Belgium and Ireland, (h) parts of Rwanda, Burundi, Uganda, Tanzania and eastern Democratic

701   Republic of Congo, near Lake Victoria, (i) the Nile Delta and Palestine, (j) the region around

702   Moscow, Russia, (k) parts of northern India, Nepal, and China, (l) southeastern China, and (m)

703   southeastern Australia, including Sydney and Melbourne.

704

705
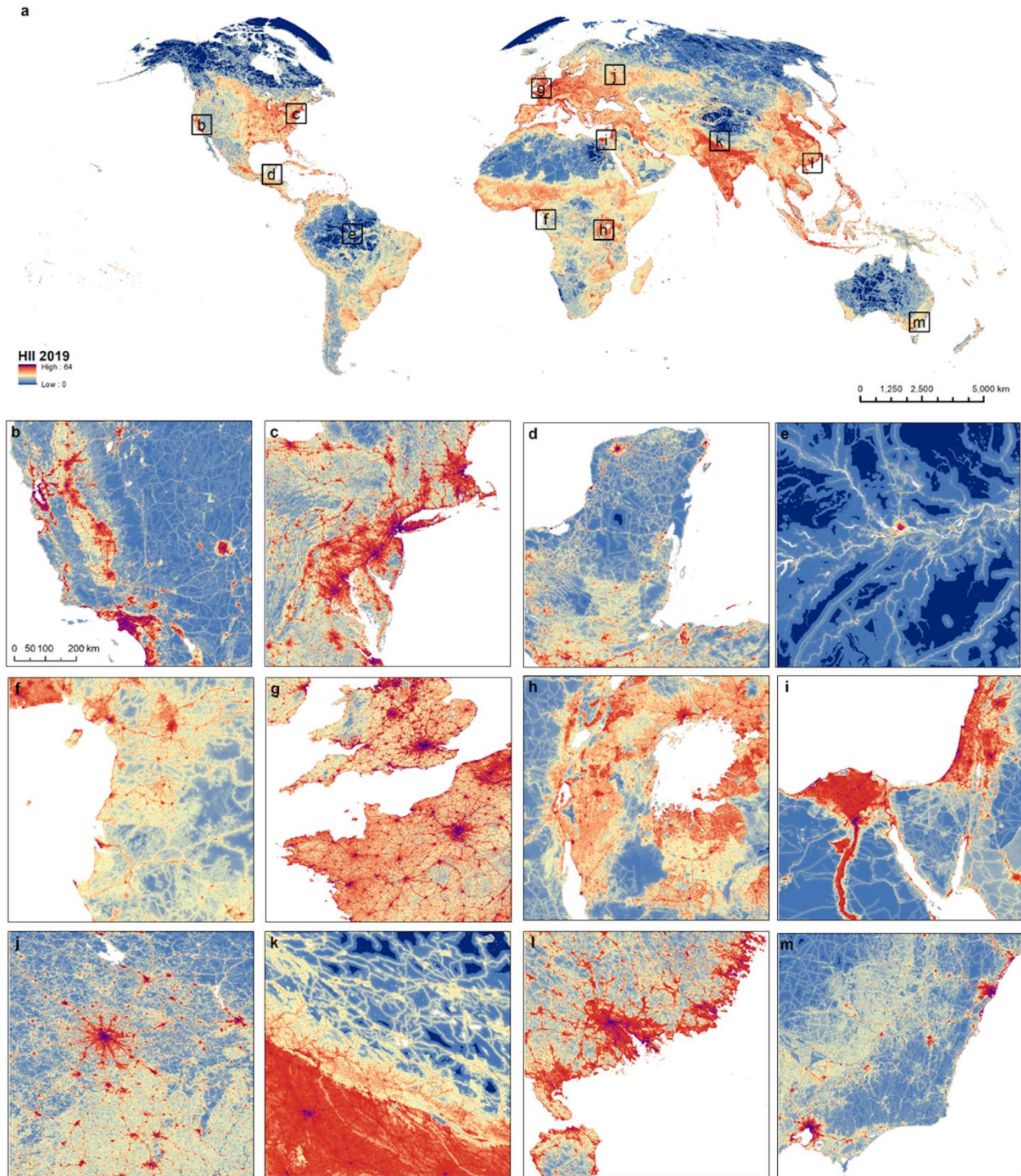
Extended Data Fig. 2. (a) Locations of detail views of the 2019 human footprint, using an

alternative color palette, illustrating (b) central California, (c) the Northeast Corridor from

Massachusetts to Virginia, (d) the Yucatan Peninsula, (e) the central Amazon Forest around
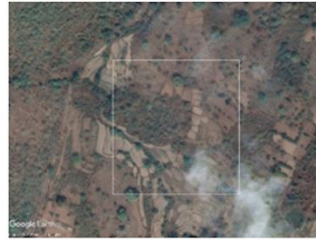
709   Manaus, Brazil, (f) parts of Nigeria, Cameroon, and Gabon along the Gulf of Guinea, (g)

710   southern England, northern France, southern England, northern France, and portions of Belgium

711   and Ireland, (h) parts of Rwanda, Burundi, Uganda, Tanzania and eastern Democratic Republic

712   of Congo, near Lake Victoria, (i) the Nile Delta and Palestine, (j) the region around Moscow,

713   Russia, (k) parts of northern India, Nepal, and China, (l) southeastern China, and (m)

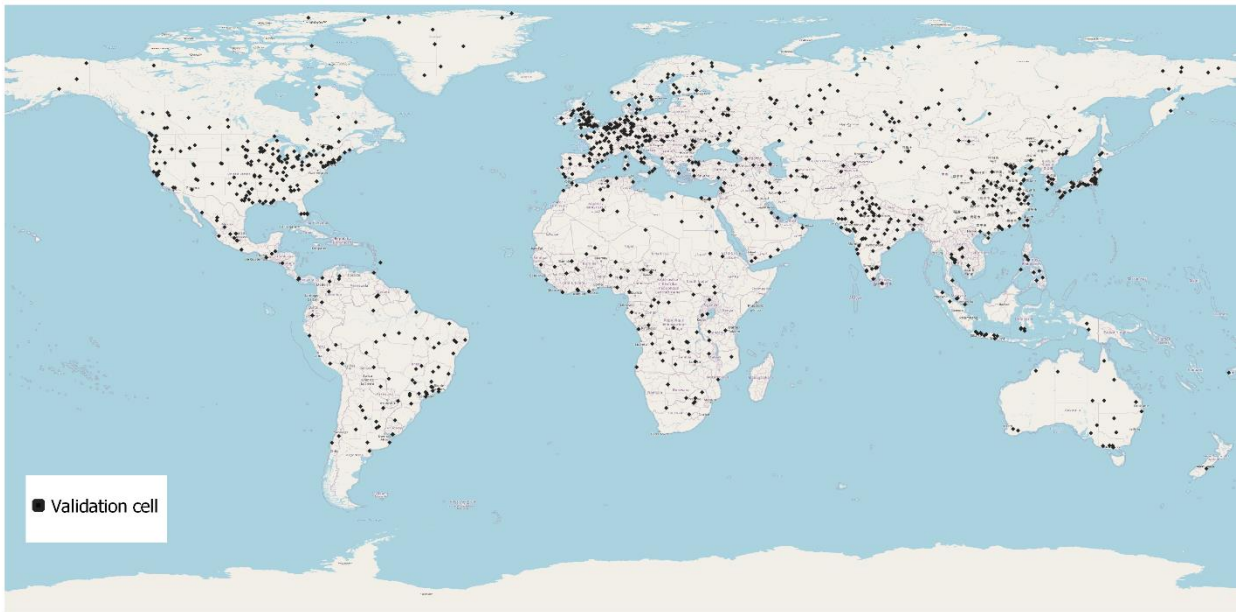714   southeastern Australia, including Sydney and Melbourne.

715

716

Extended Data Fig. 3. Stratified random sample locations used for validation of HII results.

HII = 0

HII = 0.00
Near Tapajos River, Amazonas, Brazil
2014

HII = 0.00
Near Delta Junction, Alaska, USA
2010

HII = 0.20
Near Lowman, Idaho, USA
2016

HII = 1 - 4

HII = 1.27
Near Grover, Colorado, USA
2013

HII = 2.53
Near San Justo, Argentina
2016

HII = 3.95
Near Kumboroti, Democratic Republic of the Congo
2017

HII = 5 - 10

HII = 6.17
Near Fields, Indiana, USA
2013

HII = 8.15
Near Padika, Odisha, India
2019

HII = 8.71
Near Msesia, Tanzania
2011

HII = 11 - 20

HII = 11.01
Near Des Moines, Iowa, USA
2007

Hii = 15.99
Near Xingjing, Ningxia, China
2017

HII = 19.83
Near Ambawade, Maharashtra, India
2011

HII = 21 - 30

HII = 21.04
Near Alamo Oaks, California, USA
2013

HII = 26.00
Near Aladeniya, Sri Lanka
2004

HII = 28.00
Near Shanti Nagar, Kerala, India
2013

718

Example 1 | Example 2 | Example 3

HII = 31 - 40

HII = 31.00
Near Wangqun, Jiangsu, China
2018

HII = 36.71
Near Monte Creek, British
Columbia, Canada
2019

HII = 39.24
Near Kaukauna, Wisconsin, USA
2019

HII = 41 - 50

HII = 42.00
Near Springfield, Ohio, USA
2009

HII = 45.27
Near Obaracho, Gunma, Japan
2010

HII = 50.00
Near Northside, Texas, USA
2014

HII ≥ 51

HII = 55.06
Near Oldhall, Scotland, UK
2009

HII = 61.67
Near Mentone, Victoria, Australia
20107

HII = 61.78
Near Sochi, Russia
20106

719

720 Extended Data Fig. 4. High-resolution aerial photographs illustrate different levels of Human

721 Impact Index (HII). Note that population density, power consumption/nighttime lights, and

722 distance from navigable waterways and roads are not visible in these images but do contribute to

723 the HII.

724

725
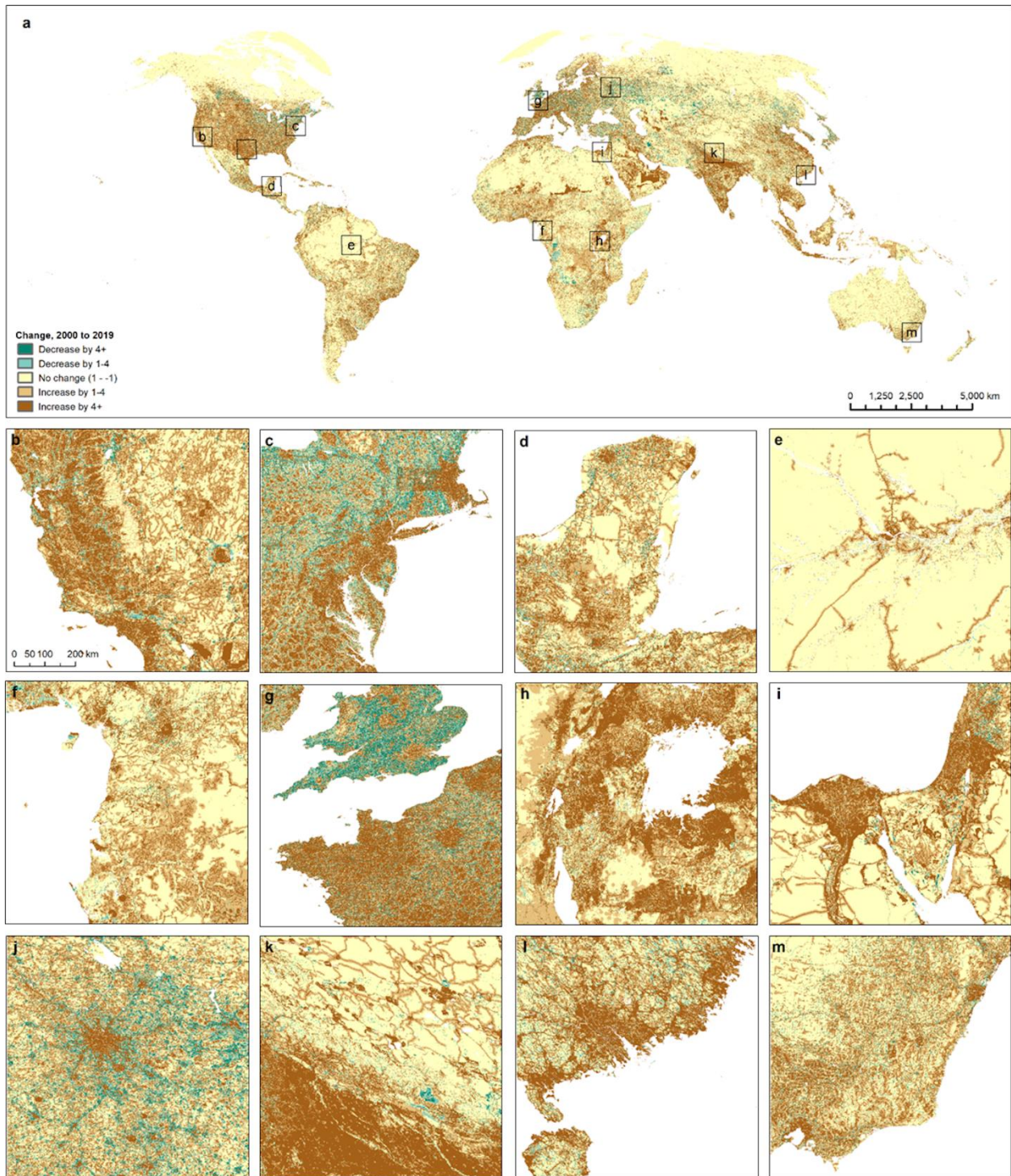
Extended Data Figure 6. (a) Locations of detail views of map of change in human footprint,

from 2000 - 2019, illustrating (b) central California, (c) the Northeast Corridor from

Massachusetts to Virginia, (d) the Yucatan Peninsula, (e) the central Amazon Forest around

729   Manaus, Brazil, (f) parts of Nigeria, Cameroon, and Gabon along the Gulf of Guinea, (g)

730   southern England and northern France, (h) parts of Rwanda, Burundi, Uganda, Tanzania and

731   eastern Democratic Republic of Congo, near Lake Victoria, (i) the Nile Delta and Palestine, (j)

732   the region around Moscow, Russia, (k) parts of northern India, Nepal, and China, (l) southeastern

733   China, and (m) southeastern Australia, including Sydney and Melbourne.

734

735
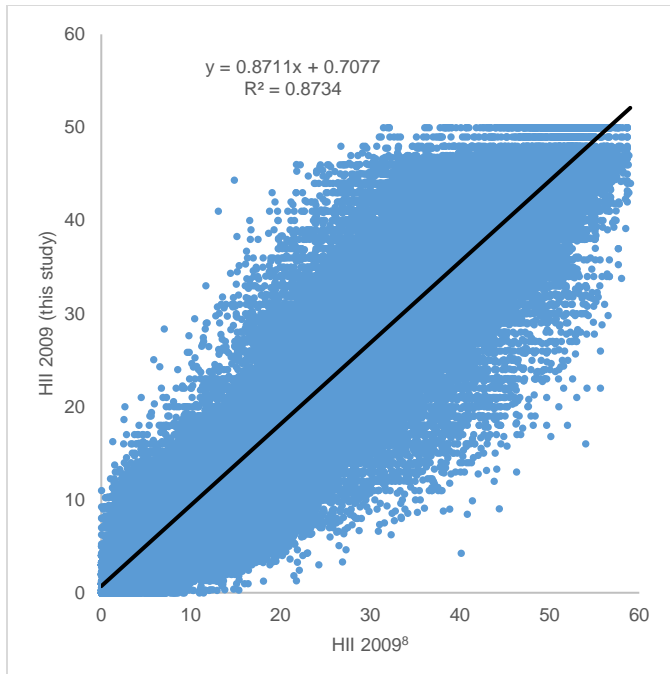
Extended Data Figure 7. Comparison of human footprint maps for 2009 between Venter et al.[8]

and this study, based on resampling our 2009 first-generation human footprint to match Venter et

al.'s 1 km cells (n = 135,726). The equation of the trendline (black) and coefficient of

determination (R^2) are shown. Note the Venter et al. data have a maximum value of 50, where in

this study, the first-generation human footprint methods have a maximum value of 59.

741 Extended Data Table 1. Summary statistics for the Human Impact Index (HII) for Anthrome 12K

742 classes[36] in 2015.

Anthrome 12K Class - Year 2015	Anthrome 12K Index Value	Count of Anthrome 12K cells	Minimum HII	Mean HII	Standard deviation HII	Maximum HII
Urban	11	10,234	2	40.02	11.7	64
Mixed settlements	12	20,963	0	20.52	11.7	63
Rice villages	21	13,976	0	23.88	8.5	63
Irrigated villages	22	27,131	1	23.96	8.5	63
Rainfed villages	23	72,244	0	21.01	8.8	63
Pastoral villages	24	11,187	0	17.72	9.1	61
Residential irrigated croplands	31	14,725	1	16.94	7.1	58
Residential rainfed croplands	32	145,532	0	15.12	6.5	58
Populated croplands	33	85,836	0	11.13	5.2	52
Remote croplands	34	42,028	0	8.73	5.2	62
Residential rangelands	41	88,626	0	11.18	5.6	57
Popuated rangelands	42	143,126	0	7.00	4.6	58
Remote rangelands	43	244,874	0	3.54	3.6	47
Residential woodlands	51	59,801	0	10.52	6.7	61
Populated woodlands	52	109,901	0	5.70	4.5	50
Remote woodlands	53	146,502	0	2.32	2.9	41
Inhabited treeless lands	54	156,930	0	5.28	5.1	62
Wild woodlands	61	328,735	0	0.89	1.8	62
Wild treeless lands	62	283,639	0	1.12	2.1	59
Uninhabited ice	63	126,453	0	0.17	0.6	15
No land	70	8	0	4.37	3.8	13

743

744

745 Extended Data Table 2. Overall accuracy and rates of commission and omission error for the

746 Human Influence Index and selected drivers, 2000 – 2019, in comparison to visual inspection of

747 high resolution aerial photography (n = 2151).

Data layer	Overall accuracy	Commission error	Omission error
HII	98.92%	1.08%	0.00%
Access from navigable waters	67.97%	6.77%	43.89%
Roads (presence and/or access)	98.04%	0.90%	1.09%
Land Cover	91.23%	4.06%	5.68%
Built Structures	69.44%	3.39%	39.04%

748

749

750 Extended Data Table 3. Most important drivers in areas where Human Influence Index (HII)

751 values dropped by 0.25/year or more, analyzed by country (n = 284)

Human Impact Driver	Percentage of countries where this driver was most important in decreasing HII values, 2000 - 2014	Percentage of countries where this driver was most important in decreasing HII values, 2015 - 2019
Built structures	0%[a]	1%
Land cover	25%	62%
Population density	11	0%
Power consumption	56%	2%
Railways	0% [a]	1%
Roads	0% [a]	28%
None[b]	7%	5%

752 a: by definition, because these drivers are represented statically.
753 b: some countries had no 300m cells with decreasing human impacts over the periods indicated.

754

755

756 Extended Data Table 4. Mean and sum of human influence index values for the countries of the

757 world in 2000 and 2019. Note Antarctica and some neighboring islands were not studied.

Country	ISO	HII Mean in 2000	HII Sum in 2000	HII Mean in 2019	HII Sum in 2019	Change in mean (2019 - 2020) %
Aruba	ABW	2,797	5.61E+06	3,712	7.44E+06	33%
Afghanistan	AFG	931	8.03E+09	1,069	9.23E+09	15%
Angola	AGO	517	7.39E+09	609	8.70E+09	18%
Anguilla	AIA	2,406	1.95E+06	3,748	3.03E+06	56%
Åland	ALA	1,070	2.89E+07	1,574	4.25E+07	47%
Albania	ALB	1,314	5.45E+08	1,595	6.62E+08	21%
Andorra	AND	1,734	1.18E+07	1,650	1.12E+07	-5%
United Arab Emirates	ARE	967	8.38E+08	1,749	1.52E+09	81%
Argentina	ARG	464	1.76E+10	651	2.46E+10	40%
Armenia	ARM	1,021	4.23E+08	1,415	5.85E+08	39%
American Samoa	ASM	1,708	4.09E+06	2,676	6.41E+06	57%
French Southern Territories	ATF	234	2.65E+07	246	2.79E+07	5%
Antigua and Barbuda	ATG	1,961	9.00E+06	2,832	1.30E+07	44%
Australia	AUS	230	2.19E+10	305	2.91E+10	33%
Austria	AUT	1,447	1.98E+09	1,991	2.72E+09	38%
Azerbaijan	AZE	1,322	1.64E+09	1,634	2.02E+09	24%
Burundi	BDI	1,914	5.35E+08	2,168	6.06E+08	13%
Belgium	BEL	2,532	1.35E+09	3,267	1.74E+09	29%
Benin	BEN	1,031	1.35E+09	1,352	1.77E+09	31%
Bonaire, Sint Eustatius and Saba	BES	1,643	5.07E+06	2,403	7.41E+06	46%
Burkina Faso	BFA	1,261	3.94E+09	1,499	4.69E+09	19%
Bangladesh	BGD	2,018	3.35E+09	2,598	4.31E+09	29%
Bulgaria	BGR	1,405	2.36E+09	1,596	2.68E+09	14%
Bahrain	BHR	2,935	2.50E+07	3,813	3.25E+07	30%
Bahamas	BHS	790	1.05E+08	952	1.27E+08	21%
Bosnia and Herzegovina	BIH	1,188	9.36E+08	1,475	1.16E+09	24%
Saint-Barthélemy	BLM	2,638	4.72E+05	3,942	7.06E+05	49%
Belarus	BLR	1,150	4.40E+09	1,449	5.55E+09	26%
Belize	BLZ	746	1.88E+08	965	2.43E+08	29%
Bermuda	BMU	2,815	1.43E+06	4,192	2.13E+06	49%
Bolivia	BOL	371	4.65E+09	558	6.99E+09	50%
Brazil	BRA	415	4.00E+10	609	5.87E+10	47%
Barbados	BRB	3,066	1.51E+07	3,773	1.85E+07	23%
Brunei	BRN	730	4.69E+07	1,000	6.42E+07	37%
Bhutan	BTN	458	2.21E+08	649	3.14E+08	42%
Bouvet Island	BVT	-	0.00E+00	-	0.00E+00	0%
Botswana	BWA	328	2.29E+09	494	3.44E+09	50%
Central African Republic	CAF	296	2.07E+09	360	2.51E+09	21%

49

Country	Code					
Canada	CAN	156	3.19E+10	202	4.13E+10	30%
Cocos Islands	CCK	1,097	1.30E+05	1,908	2.27E+05	74%
Switzerland	CHE	1,646	1.06E+09	2,187	1.41E+09	33%
Chile	CHL	418	4.37E+09	569	5.95E+09	36%
China	CHN	815	1.05E+11	1,024	1.33E+11	26%
Côte d'Ivoire	CIV	1,105	3.99E+09	1,330	4.80E+09	20%
Cameroon	CMR	675	3.52E+09	895	4.67E+09	32%
Democratic Republic of the Congo	COD	561	1.45E+10	751	1.93E+10	34%
Republic of Congo	COG	463	1.76E+09	567	2.15E+09	22%
Cook Islands	COK	1,485	3.88E+06	1,918	5.01E+06	29%
Colombia	COL	519	6.57E+09	682	8.64E+09	31%
Comoros	COM	1,520	2.80E+07	1,925	3.54E+07	27%
Cape Verde	CPV	1,562	7.14E+07	1,948	8.91E+07	25%
Costa Rica	CRI	1,121	6.48E+08	1,368	7.90E+08	22%
Cuba	CUB	1,341	1.74E+09	1,619	2.10E+09	21%
Curaçao	CUW	2,217	1.05E+07	2,964	1.41E+07	34%
Christmas Island	CXR	1,068	1.58E+06	1,514	2.24E+06	42%
Cayman Islands	CYM	1,895	5.74E+06	2,634	7.98E+06	39%
Cyprus	CYP	1,633	1.26E+08	2,115	1.63E+08	29%
Czech Republic	CZE	1,895	2.54E+09	2,292	3.08E+09	21%
Germany	DEU	2,011	1.26E+10	2,492	1.56E+10	24%
Djibouti	DJI	1,036	2.56E+08	1,199	2.96E+08	16%
Dominica	DMA	1,125	9.64E+06	1,835	1.57E+07	63%
Denmark	DNK	1,911	1.59E+09	2,463	2.06E+09	29%
Dominican Republic	DOM	1,279	7.19E+08	1,587	8.92E+08	24%
Algeria	DZA	264	7.74E+09	390	1.14E+10	48%
Ecuador	ECU	653	1.85E+09	996	2.82E+09	53%
Egypt	EGY	308	3.76E+09	423	5.16E+09	37%
Eritrea	ERI	1,038	1.44E+09	1,122	1.56E+09	8%
Western Sahara	ESH	101	3.33E+08	200	6.57E+08	97%
Spain	ESP	1,330	9.76E+09	1,681	1.23E+10	26%
Estonia	EST	818	7.53E+08	1,364	1.25E+09	67%
Ethiopia	ETH	963	1.22E+10	1,138	1.45E+10	18%
Finland	FIN	543	4.22E+09	939	7.31E+09	73%
Fiji	FJI	867	1.88E+08	1,162	2.52E+08	34%
Falkland Islands	FLK	305	6.31E+07	474	9.81E+07	56%
France	FRA	1,682	1.48E+10	2,353	2.07E+10	40%
Faroe Islands	FRO	1,285	4.35E+07	1,469	4.98E+07	14%
Micronesia	FSM	1,155	8.53E+06	1,783	1.32E+07	54%
Gabon	GAB	355	1.04E+09	553	1.62E+09	56%
United Kingdom	GBR	1,850	8.45E+09	2,007	9.16E+09	8%
Georgia	GEO	940	9.81E+08	1,195	1.25E+09	27%
Guernsey	GGY	3,172	4.15E+06	3,685	4.83E+06	16%
Ghana	GHA	1,191	3.14E+09	1,509	3.97E+09	27%
Gibraltar	GIB	4,204	3.32E+05	4,931	3.90E+05	17%

Guinea	GIN	1,028	2.86E+09	1,164	3.24E+09	13%
Guadeloupe	GLP	2,043	3.81E+07	3,003	5.60E+07	47%
Gambia	GMB	1,698	2.04E+08	1,868	2.24E+08	10%
Guinea-Bissau	GNB	1,111	4.22E+08	1,203	4.57E+08	8%
Equatorial Guinea	GNQ	837	2.51E+08	1,034	3.10E+08	24%
Greece	GRC	1,465	2.72E+09	1,788	3.32E+09	22%
Grenada	GRD	1,883	7.30E+06	2,774	1.08E+07	47%
Greenland	GRL	13	1.17E+09	14	1.20E+09	2%
Guatemala	GTM	1,164	1.46E+09	1,440	1.81E+09	24%
French Guiana	GUF	115	1.06E+08	207	1.91E+08	80%
Guam	GUM	1,884	1.14E+07	2,837	1.71E+07	51%
Guyana	GUY	132	3.10E+08	182	4.26E+08	37%
Hong Kong	HKG	2,797	3.42E+07	3,766	4.61E+07	35%
Heard Island and McDonald Islands	HMD	46	3.00E+05	2	1.35E+04	-95%
Honduras	HND	804	1.04E+09	1,078	1.39E+09	34%
Croatia	HRV	1,453	1.28E+09	1,832	1.62E+09	26%
Haiti	HTI	1,465	4.62E+08	1,985	6.26E+08	35%
Hungary	HUN	1,771	2.66E+09	2,030	3.04E+09	15%
Indonesia	IDN	804	1.68E+10	1,189	2.49E+10	48%
Isle of Man	IMN	2,202	2.36E+07	2,298	2.46E+07	4%
India	IND	1,660	6.33E+10	2,184	8.33E+10	32%
British Indian Ocean Territory	IOT	943	3.23E+05	1,703	5.83E+05	81%
Ireland	IRL	1,361	1.73E+09	1,738	2.21E+09	28%
Iran	IRN	996	2.13E+10	1,177	2.52E+10	18%
Iraq	IRQ	940	5.51E+09	1,245	7.30E+09	32%
Iceland	ISL	278	7.06E+08	438	1.11E+09	58%
Israel	ISR	1,699	4.81E+08	2,229	6.31E+08	31%
Italy	ITA	1,567	7.07E+09	2,222	1.00E+10	42%
Jamaica	JAM	1,693	2.17E+08	2,071	2.66E+08	22%
Jersey	JEY	3,524	6.98E+06	3,645	7.22E+06	3%
Jordan	JOR	595	6.88E+08	844	9.76E+08	42%
Japan	JPN	1,760	9.07E+09	1,973	1.02E+10	12%
Kazakhstan	KAZ	562	2.50E+10	597	2.66E+10	6%
Kenya	KEN	866	5.57E+09	1,111	7.14E+09	28%
Kyrgyzstan	KGZ	890	2.52E+09	998	2.83E+09	12%
Cambodia	KHM	942	1.92E+09	1,281	2.60E+09	36%
Kiribati	KIR	979	7.46E+06	1,524	1.16E+07	56%
Saint Kitts and Nevis	KNA	2,184	6.37E+06	2,879	8.40E+06	32%
South Korea	KOR	1,881	2.55E+09	2,292	3.11E+09	22%
Kuwait	KWT	1,495	3.31E+08	1,992	4.41E+08	33%
Laos	LAO	724	1.95E+09	962	2.59E+09	33%
Lebanon	LBN	2,233	3.06E+08	2,606	3.57E+08	17%
Liberia	LBR	1,102	1.19E+09	1,295	1.39E+09	17%
Libya	LBY	240	4.86E+09	289	5.86E+09	21%
Saint Lucia	LCA	1,696	1.16E+07	2,505	1.71E+07	48%

Liechtenstein	LIE	1,892	4.97E+06	2,522	6.63E+06	33%
Sri Lanka	LKA	1,646	1.21E+09	2,087	1.53E+09	27%
Lesotho	LSO	1,139	4.46E+08	1,702	6.66E+08	49%
Lithuania	LTU	1,262	1.57E+09	1,785	2.22E+09	41%
Luxembourg	LUX	2,143	9.48E+07	2,826	1.25E+08	32%
Latvia	LVA	883	1.14E+09	1,435	1.85E+09	63%
Macao	MAC	3,472	9.76E+05	5,225	1.47E+06	51%
Saint-Martin	MAF	2,817	1.44E+06	3,942	2.01E+06	40%
Morocco	MAR	820	4.45E+09	1,084	5.87E+09	32%
Monaco	MCO	4,578	9.16E+04	6,063	1.21E+05	32%
Moldova	MDA	1,741	9.55E+08	2,026	1.11E+09	16%
Madagascar	MDG	925	6.46E+09	1,061	7.41E+09	15%
Maldives	MDV	1,632	1.96E+06	2,986	3.59E+06	83%
Mexico	MEX	583	1.39E+10	790	1.88E+10	36%
Marshall Islands	MHL	1,293	1.69E+06	1,876	2.46E+06	45%
Macedonia	MKD	1,334	4.83E+08	1,525	5.51E+08	14%
Mali	MLI	456	6.69E+09	619	9.07E+09	36%
Malta	MLT	3,317	1.38E+07	4,554	1.89E+07	37%
Myanmar	MMR	1,007	8.01E+09	1,196	9.52E+09	19%
Montenegro	MNE	1,026	2.03E+08	1,413	2.79E+08	38%
Mongolia	MNG	236	5.94E+09	290	7.31E+09	23%
Northern Mariana Islands	MNP	1,164	6.16E+06	1,869	9.88E+06	61%
Mozambique	MOZ	663	6.04E+09	905	8.25E+09	37%
Mauritania	MRT	215	2.66E+09	250	3.10E+09	16%
Montserrat	MSR	1,123	1.27E+06	1,557	1.76E+06	39%
Martinique	MTQ	2,226	2.78E+07	3,267	4.07E+07	47%
Mauritius	MUS	2,381	5.57E+07	2,969	6.94E+07	25%
Malawi	MWI	1,235	1.34E+09	1,751	1.90E+09	42%
Malaysia	MYS	783	2.87E+09	1,138	4.17E+09	45%
Mayotte	MYT	1,851	7.63E+06	2,714	1.12E+07	47%
Namibia	NAM	213	2.12E+09	349	3.46E+09	63%
New Caledonia	NCL	735	1.62E+08	918	2.02E+08	25%
Niger	NER	347	4.82E+09	460	6.38E+09	32%
Norfolk Island	NFK	1,660	8.27E+05	2,775	1.38E+06	67%
Nigeria	NGA	1,363	1.40E+10	1,671	1.72E+10	23%
Nicaragua	NIC	893	1.21E+09	1,053	1.43E+09	18%
Niue	NIU	1,079	3.33E+06	1,284	3.96E+06	19%
Netherlands	NLD	2,576	1.59E+09	3,267	2.02E+09	27%
Norway	NOR	569	4.37E+09	781	6.00E+09	37%
Nepal	NPL	989	1.84E+09	1,433	2.67E+09	45%
Nauru	NRU	2,283	5.32E+05	4,121	9.60E+05	80%
New Zealand	NZL	530	2.07E+09	690	2.70E+09	30%
Oman	OMN	381	1.41E+09	756	2.79E+09	98%
Pakistan	PAK	1,330	1.49E+10	1,492	1.67E+10	12%
Panama	PAN	819	6.85E+08	969	8.10E+08	18%

Pitcairn Islands	PCN	1,021	6.39E+05	1,139	7.13E+05	11%
Peru	PER	433	6.29E+09	578	8.41E+09	34%
Philippines	PHL	1,302	4.31E+09	1,769	5.86E+09	36%
Palau	PLW	935	4.32E+06	1,539	7.11E+06	65%
Papua New Guinea	PNG	434	2.24E+09	545	2.81E+09	26%
Poland	POL	1,735	9.63E+09	2,145	1.19E+10	24%
Puerto Rico	PRI	2,286	2.38E+08	3,147	3.27E+08	38%
North Korea	PRK	1,131	2.00E+09	1,428	2.52E+09	26%
Portugal	PRT	1,199	1.58E+09	1,716	2.26E+09	43%
Paraguay	PRY	487	2.35E+09	753	3.63E+09	55%
Palestina	PSE	2,201	1.74E+08	2,940	2.32E+08	34%
French Polynesia	PYF	1,261	4.53E+07	1,543	5.54E+07	22%
Qatar	QAT	1,090	1.56E+08	2,174	3.11E+08	99%
Reunion	REU	1,827	5.42E+07	2,604	7.73E+07	43%
Romania	ROU	1,445	5.44E+09	1,668	6.28E+09	15%
Russia	RUS	241	9.36E+10	296	1.15E+11	23%
Rwanda	RWA	1,549	4.12E+08	2,145	5.71E+08	38%
Saudi Arabia	SAU	540	1.27E+10	863	2.03E+10	60%
Sudan	SDN	698	1.52E+10	802	1.75E+10	15%
Senegal	SEN	1,253	2.82E+09	1,400	3.15E+09	12%
Singapore	SGP	3,159	2.24E+07	4,557	3.23E+07	44%
South Georgia and the South Sandwich Islands	SGS	201	1.23E+07	178	1.09E+07	-12%
Saint Helena	SHN	844	4.02E+06	1,014	4.83E+06	20%
Svalbard and Jan Mayen	SJM	4	1.42E+07	16	5.41E+07	280%
Solomon Islands	SLB	473	1.45E+08	771	2.37E+08	63%
Sierra Leone	SLE	1,436	1.17E+09	1,622	1.32E+09	13%
El Salvador	SLV	1,536	3.56E+08	1,867	4.32E+08	22%
San Marino	SMR	2,753	2.59E+06	3,880	3.65E+06	41%
Somalia	SOM	1,019	7.27E+09	1,055	7.52E+09	3%
Saint Pierre and Miquelon	SPM	899	2.89E+06	1,155	3.71E+06	28%
Serbia	SRB	1,468	1.77E+09	1,731	2.08E+09	18%
South Sudan	SSD	674	4.77E+09	842	5.96E+09	25%
São Tomé and Príncipe	STP	1,207	1.34E+07	1,574	1.74E+07	30%
Suriname	SUR	114	1.84E+08	190	3.08E+08	67%
Slovakia	SVK	1,666	1.37E+09	1,933	1.59E+09	16%
Slovenia	SVN	1,374	4.39E+08	1,854	5.92E+08	35%
Sweden	SWE	568	5.64E+09	838	8.32E+09	48%
Swaziland	SWZ	1,172	2.54E+08	1,896	4.10E+08	62%
Sint Maarten	SXM	3,134	1.12E+06	4,305	1.54E+06	37%
Seychelles	SYC	1,735	7.99E+06	2,187	1.01E+07	26%
Syria	SYR	1,166	2.95E+09	1,383	3.50E+09	19%
Turks and Caicos Islands	TCA	887	8.60E+06	1,156	1.12E+07	30%
Chad	TCD	467	6.88E+09	638	9.40E+09	37%
Togo	TGO	1,166	7.50E+08	1,514	9.74E+08	30%

Thailand	THA	1,449	8.56E+09	1,955	1.15E+10	35%
Tajikistan	TJK	799	1.59E+09	949	1.89E+09	19%
Tokelau	TKL	1,418	8.93E+04	1,549	9.76E+04	9%
Turkmenistan	TKM	757	5.06E+09	927	6.20E+09	22%
Timor-Leste	TLS	1,283	2.16E+08	1,550	2.60E+08	21%
Tonga	TON	1,624	1.24E+07	2,246	1.72E+07	38%
Trinidad and Tobago	TTO	1,678	9.70E+07	2,321	1.34E+08	38%
Tunisia	TUN	976	2.03E+09	1,207	2.51E+09	24%
Turkey	TUR	1,293	1.43E+10	1,575	1.74E+10	22%
Tuvalu	TUV	1,163	2.59E+05	2,221	4.95E+05	91%
Taiwan	TWN	1,601	7.00E+08	2,226	9.74E+08	39%
Tanzania	TZA	835	8.32E+09	1,147	1.14E+10	37%
Uganda	UGA	1,261	2.90E+09	1,772	4.07E+09	41%
Ukraine	UKR	1,471	1.46E+10	1,718	1.71E+10	17%
United States Minor Outlying Islands	UMI	605	1.79E+05	1,244	3.68E+05	106%
Uruguay	URY	485	1.12E+09	613	1.41E+09	26%
United States	USA	607	8.99E+10	902	1.33E+11	48%
Uzbekistan	UZB	962	6.23E+09	1,154	7.47E+09	20%
Vatican City	VAT	5,056	4.55E+04	5,900	5.31E+04	17%
Saint Vincent and the Grenadines	VCT	1,731	7.47E+06	2,213	9.55E+06	28%
Venezuela	VEN	546	5.55E+09	696	7.07E+09	27%
British Virgin Islands	VGB	2,083	3.03E+06	2,890	4.21E+06	39%
Virgin Islands, U.S.	VIR	2,870	1.09E+07	3,710	1.41E+07	29%
Vietnam	VNM	1,394	5.28E+09	1,799	6.81E+09	29%
Vanuatu	VUT	718	9.96E+07	869	1.21E+08	21%
Wallis and Futuna	WLF	1,687	2.14E+06	2,346	2.98E+06	39%
Samoa	WSM	1,273	4.09E+07	1,600	5.14E+07	26%
Akrotiri and Dhekelia	XAD	2,408	7.33E+06	3,028	9.22E+06	26%
Caspian Sea	XCA	894	1.21E+07	1,144	1.55E+07	28%
Kosovo	XKO	1,543	2.54E+08	2,026	3.33E+08	31%
Northern Cyprus	XNC	1,681	7.50E+07	2,045	9.13E+07	22%
Paracel Islands	XPI	1,765	7.06E+04	2,696	1.08E+05	53%
Spratly Islands	XSP	175	1.93E+03	1,489	1.64E+04	748%
Yemen	YEM	527	2.77E+09	677	3.56E+09	29%
South Africa	ZAF	684	1.06E+10	771	1.20E+10	13%
Zambia	ZMB	594	5.05E+09	802	6.81E+09	35%
Zimbabwe	ZWE	1,006	4.61E+09	1,358	6.22E+09	35%

758

759